

สมบัติเชิงกลและการประยุกต์ใช้ของคอนกรีตเสริมเส้นใยอะรามิด

นางสาวชุง ที เหยียน



จุฬาลงกรณ์มหาวิทยาลัย
CHULALONGKORN UNIVERSITY

บทคัดย่อและแฟ้มข้อมูลฉบับเต็มของวิทยานิพนธ์ตั้งแต่ปีการศึกษา 2554 ที่ให้บริการในคลังปัญญาจุฬาฯ (CUIR)

เป็นแฟ้มข้อมูลของนิสิตเจ้าของวิทยานิพนธ์ ที่ส่งผ่านทางบัณฑิตวิทยาลัย

The abstract and full text of theses from the academic year 2011 in Chulalongkorn University Intellectual Repository (CUIR)

วิทยานิพนธ์นี้เป็นส่วนหนึ่งของการศึกษาตามหลักสูตรปริญญาวิทยาศาสตรมหาบัณฑิต

สาขาวิชาวิศวกรรมโยธา ภาควิชาวิศวกรรมโยธา

คณะวิศวกรรมศาสตร์ จุฬาลงกรณ์มหาวิทยาลัย

ปีการศึกษา 2558

ลิขสิทธิ์ของจุฬาลงกรณ์มหาวิทยาลัย

MECHANICAL PROPERTIES AND APPLICATION OF ARAMID FIBER REINFORCED
CONCRETE

Miss Chung Thi Nguyen



A Thesis Submitted in Partial Fulfillment of the Requirements
for the Degree of Master of Engineering Program in Civil Engineering

Department of Civil Engineering

Faculty of Engineering

Chulalongkorn University

Academic Year 2015

Copyright of Chulalongkorn University

Thesis Title	MECHANICAL PROPERTIES AND APPLICATION OF ARAMID FIBER REINFORCED CONCRETE
By	Miss Chung Thi Nguyen
Field of Study	Civil Engineering
Thesis Advisor	Pitcha Jongvivatsakul, Ph.D.

Accepted by the Faculty of Engineering, Chulalongkorn University in Partial
Fulfillment of the Requirements for the Master's Degree

.....Dean of the Faculty of Engineering
(Associate Professor Supot Teachavorasinskun, Ph.D.)

THESIS COMMITTEE

.....Chairman
(Associate Professor Akhrawat Lenwari, Ph.D.)

.....Thesis Advisor
(Pitcha Jongvivatsakul, Ph.D.)

.....Examiner
(Associate Professor Withit Pansuk, Ph.D.)

.....External Examiner
(Ganchai Tanapornraweekit, Ph.D.)

ชุง ที เหยียน : สมบัติเชิงกลและการประยุกต์ใช้ของคอนกรีตเสริมเส้นใยอะรามิด (MECHANICAL PROPERTIES AND APPLICATION OF ARAMID FIBER REINFORCED CONCRETE) อ.ที่ปรึกษาวิทยานิพนธ์หลัก: พิชชา จองวิวัฒน์สกุล, 85 หน้า.

การกักความร้อนของเหล็กเสริมเป็นสาเหตุของการเสื่อมสภาพของโครงสร้างคอนกรีตเสริมเหล็กอันจะส่งผลให้กำลังรับแรงและความทนทานของโครงสร้างลดลง เส้นใยอะรามิดเป็นเส้นใยสังเคราะห์ที่มีกำลังรับแรงดึงสูงและมีความทนทานต่อการกัดกร่อนสูง งานวิจัยนี้มีวัตถุประสงค์เพื่อศึกษาอิทธิพลของเส้นใยอะรามิดและอิทธิพลของความยาวและรูปร่างของเส้นใยอะรามิดต่อสมบัติเชิงกลของคอนกรีตเสริมเส้นใยอะรามิด นอกจากนี้ยังศึกษาพฤติกรรมการรับแรงดัดของคานคอนกรีตเสริมเหล็กที่ถูกกักความร้อนและซ่อมแซมด้วยคอนกรีตเสริมเส้นใยอะรามิดเปรียบเทียบกับ การซ่อมแซมด้วยผลิตภัณฑ์มอร์ตาร์

การทดสอบสมบัติเชิงกลของคอนกรีตและคอนกรีตเสริมเส้นใยอะรามิด ประกอบด้วย การทดสอบกำลังรับแรงอัด การทดสอบกำลังรับแรงดึงโดยวิธีผ่าซีก และการทดสอบกำลังรับแรงดึงโดยตรง เส้นใยอะรามิดที่นำมาทดสอบมี 5 ชนิดซึ่งมีความยาวและรูปร่างที่แตกต่างกัน โดยมีความยาว 30 40 และ 50 มิลลิเมตร มีรูปร่างเป็นแบบตรงและแบบเกลียว ปริมาณเส้นใยที่ใช้คือ 1 เปอร์เซ็นต์โดยปริมาตร จากผลการทดสอบพบว่ากำลังรับแรงดึงโดยวิธีผ่าซีกเพิ่มขึ้นอย่างมีนัยสำคัญเมื่อเสริมเส้นใยอะรามิดในคอนกรีต เช่นเดียวกันกับกำลังรับแรงดึงโดยตรงซึ่งพบว่าคอนกรีตเสริมเส้นใยอะรามิดมีกำลังรับแรงดึงหลังจากเกิดรอยร้าวที่ดีขึ้น นอกจากนี้ความยาวและรูปร่างของเส้นใยส่งผลต่อพฤติกรรมการรับแรงดัดของคอนกรีตเสริมเส้นใยอะรามิด โดยความยาว 40 มิลลิเมตรเป็นความยาวที่เหมาะสมและสามารถเพิ่มกำลังรับแรงดัดของคอนกรีตเสริมเส้นใยได้ เมื่อพิจารณาถึงอิทธิพลของรูปร่างพบว่าเส้นใยแบบตรงให้ค่าความเค้นดึงสูงสุดมากกว่า ในทางกลับกันเส้นใยแบบเกลียวให้กำลังรับแรงดัดในช่วงหลังจากการเกิดรอยแตกที่มากกว่า

ในส่วนที่สอง คานคอนกรีตเสริมเหล็กจำนวนสี่คานถูกทดสอบภายใต้แรงกระทำแบบสี่จุด ประกอบด้วยคานควบคุมที่ไม่เกิดการกักความร้อนและคานที่เกิดการกักความร้อนด้วยวิธีเร่งกระแสไฟฟ้าจากระดับการกักความร้อนเท่ากับ 10% จำนวนสามคาน จากนั้นได้ซ่อมแซมในบริเวณที่เกิดการกักความร้อนด้วยมอร์ตาร์เสริมเส้นใยอะรามิดและผลิตภัณฑ์มอร์ตาร์ที่มีจำหน่ายในท้องตลาด โดยเส้นใยอะรามิดที่ใช้เป็นแบบเกลียวมีความยาว 40 มิลลิเมตร จากผลการทดสอบพบว่ากำลังรับแรงดัดของคานคอนกรีตเสริมเหล็กที่ถูกกักความร้อนกลับมามีค่าใกล้เคียงกับคานที่ไม่เกิดการกักความร้อนเมื่อซ่อมแซมด้วยมอร์ตาร์เสริมเส้นใยอะรามิด และพบว่าความกว้างของรอยร้าวเนื่องจากแรงดัดมีค่าลดลง อย่างไรก็ตามกำลังรับแรงดัดของคานกลับไม่เพิ่มขึ้นเมื่อซ่อมแซมด้วยผลิตภัณฑ์มอร์ตาร์ที่มีจำหน่ายในท้องตลาด นอกจากนี้ผู้วิจัยได้นำเสนอแบบจำลองเพื่อทำนายกำลังรับแรงดัดของคาน พบว่าผลการทำนายใกล้เคียงกับผลการทดลอง ดังนั้นแบบจำลองที่นำเสนอสามารถใช้ในการทำนายกำลังรับแรงดัดของคานได้

ภาควิชา วิศวกรรมโยธา

สาขาวิชา วิศวกรรมโยธา

ปีการศึกษา 2558

ลายมือชื่อนิสิต

ลายมือชื่อ อ.ที่ปรึกษาหลัก

5770516021 : MAJOR CIVIL ENGINEERING

KEYWORDS: ARAMID FIBER / FIBER REINFORCED CONCRETE / FIBER GEOMETRY / DIRECT TENSILE TEST / ACCELERATED CORROSION / FLEXURAL BEHAVIORS RC BEAM

CHUNG THI NGUYEN: MECHANICAL PROPERTIES AND APPLICATION OF ARAMID FIBER REINFORCED CONCRETE. ADVISOR: PITCHA JONGVIVATSAKUL, Ph.D., 85 pp.

Corrosion of reinforcement is one of the main cause of deterioration of reinforced concrete (RC) structures which affects the load carrying capacity and durability of structures. Aramid fibers are known as synthetic fibers that have excellent tensile strength and high corrosion resistance. The purposes of this study are to investigate the effect of the presence of fibers and fiber geometry on mechanical properties of aramid fiber reinforced concrete (ARFC) and to investigate the flexural behaviour of corroded RC beams which were repaired by aramid fiber reinforced mortar and mortar product in the market.

To accomplish the first objective, compressive, splitting, and direct tensile tests were conducted. Plain concrete and five fiber types of aramid fiber reinforced concrete having the different shape and length were tested. Fiber lengths were 30, 40 and 50 mm. Fibers were single and twisted shape. The volume fraction of fibers was 1.0% in all AFRC mixes. Significant improvement of splitting tensile strength was observed with the presence of aramid fibers. Especially for direct tensile strength, aramid fibers could provide better post-cracking tensile resistance. The length and shape of aramid fibers strongly affect the tensile behaviour of AFRC. Forty millimeter is the proper fiber length to increase the tensile strength. Although the single shape fibers yields the highest peak tensile stress, twisted fibers can resist higher load in post-peak region.

In the second part, four reinforced concrete beams were tested under four point bending. One beams was control beam without corrosion and three beams were corroded by accelerate corrosion to reach 10% mass loss of longitudinal reinforcement. Two corroded beams were repaired at the tensile zone by aramid fiber reinforced mortar (AFRM) and mortar product in the market. The aramid fibers used are 40-mm-twisted fibers. The results showed that the load capacity of the corroded RC beam repairing by AFRM was recovered to be close to the non-corroded RC beam. The width of cracks in corroded beam repairing by AFRM decreases significantly. However, the flexural capacity of corroded RC beams could not be recovered when it was repaired by mortar only. Finally, a model was suggested to predict the flexural capacity of beams. The predicted results from the model are found to agree well with test data obtained. It shows that the flexural capacity of beams can be suggested by the predict model accurately.

Department: Civil Engineering

Student's Signature

Field of Study: Civil Engineering

Advisor's Signature

Academic Year: 2015

ACKNOWLEDGEMENTS

This research was carried out at the Laboratory for Concrete and Materials Testing, Department of Civil Engineering, Chulalongkorn University (CU). It was funded by AUN/ Southeast Asia Engineering Education Development Network (AUN/SEED-Net) scholarship.

First of all, I would like to express my deepest gratitude to my thesis advisor Dr. Pitcha Jongvivatsakul for her empathy, guidance, support and patience during the development of this research. I have been extremely lucky to have an advisor who cared so much about my work, and who responded to my questions and queries so promptly.

I wish to thank to the thesis defense committee for the time and effort which they put into reading and judging the thesis and for their valuable comments: Assoc. Prof. Akharawat Lenwari, Ph.D., Assoc. Prof. Withit Pansuk, Ph.D., and Dr. Ganchai Tanapornraweekit. I would like to give a special thank Dr. Ganchai for his support during the experimental progress.

Much of the experimental program of this thesis could not have been conducted without the help of the technicians and engineers of our laboratory. They made much of the experimental program possible with their great experience, availability and patience.

I would like to thank my colleagues for their friendship, their help and their cooperation. First of all, I would like to sincerely thank Mr. Buble for his help, support of this research. I would also like to thank Mss. Grace Tug for her advice, her support, and our discussion. Finally, I would like to express my thanks to Mr. Thi, Mr. Thuc, Mr. Pamuko, and Mss. Htet for all of their advice, their support, and their encouragement.

Last but not least, I would like to thank my beloved family for their unconditional support, encouragement and help.

CONTENTS

	Page
THAI ABSTRACT	iv
ENGLISH ABSTRACT	v
ACKNOWLEDGEMENTS	vi
CONTENTS	vii
Chapter 1 INTRODUCTION.....	5
1.1 General	5
1.2 Objectives of the research	6
1.3 Scopes of the thesis	7
1.4 Thesis outline.....	7
Chapter 2 LITERATURE REVIEW	10
2.1 Fiber Reinforced Concrete (FRC).....	10
2.2 Synthetic fiber.....	12
2.3 Aramid fibers	13
2.4 Corrosion.....	15
2.4.1 General.....	15
2.4.2 Accelerated corrosion	16
2.4.3 The effect of corrosion on RC beams	17
2.4.3.1 Bond strength.....	18
2.4.3.2 Corrosion crack patterns and widths.....	19
2.4.3.3 Flexural capacity.....	20
2.4.4 The effects of corrosion on reinforced concrete with fibers addition.....	20
2.5 Mechanical of fiber reinforced concrete	22

	Page
2.5.1 Tensile strength of fiber reinforced concrete	22
2.5.2 Ultra high strength fiber reinforced concrete using aramid fiber	24
2.6 Repairing reinforced beam by fibers reinforced concrete	25
2.7 Modelling of flexural capacity of RC beams.....	26
Chapter 3 EXPERIMENTAL PROGRAM.....	31
3.1 General	31
3.2 Mechanical properties of aramid fibers reinforced concrete	32
3.2.1 Material and mix-design	32
3.2.2 Specimens	34
3.2.3 Experimental equipment and test procedures	35
3.2.3.1 Compressive and splitting test	35
3.2.3.2 Direct tensile test	35
3.3 Flexural repairing of corroded RC beams by aramid fiber mortar and market product	36
3.3.1 Material properties	36
3.3.1.1 Concrete	36
3.3.1.2 Steel reinforcement	36
3.3.1.3 Aramid fibers reinforced mortar	37
3.3.1.4 Market product	38
3.3.2 Specimen layout and detail	39
3.3.3 Accelerated corrosion test.....	40
3.3.4 Repairing procedures.....	41
3.3.4.1 Breaking damaged concrete	41

	Page
3.3.4.2 Soaking corroded reinforcement.....	41
3.3.4.3 Repairing beams by AFRC and product available in market ...	42
3.3.5 Test set up	43
Chapter 4 EXPERIMENTAL RESULTS AND DISCUSSION	45
4.1 General	45
4.2 Mechanical properties of aramid fibers reinforced concrete.....	46
4.2.1 Compression and splitting strength	46
4.2.2 Direct tensile strength.....	48
4.3 Test results and discussion of RC Beams.....	53
4.3.1 Accelerated corrosion result	53
4.3.1.1 Concrete damage condition.....	53
4.3.1.2 Steel damage condition.....	55
4.3.2 Flexural repairing RC beams	56
4.3.2.1 Load- deflection behaviour and failure mode.....	56
4.3.2.2 Ductility index	62
4.3.2.3 Cracks pattern	63
4.3.2.4 Width of crack.....	66
Chapter 5 PREDICTION OF FLEXURAL STRENGTH OF REPAIRING BEAMS.....	70
5.2 Material model	70
5.3 Methodology.....	72
Chapter 6 CONCLUSION AND RECOMMENDATION.....	77
6.1 Experiment Result.....	77
6.1.1 Mechanical properties AFRC test.....	77

	Page
6.1.2 Flexural behaviour of reinforced concrete beam.....	78
6.2 Recommendations for future work	79
REFERENCES	83
VITA.....	85



LIST OF FIGURES

Figure 1.1 Products of aramid fibers [1]	5
Figure 1.2 Outline of thesis.....	9
Figure 2.1 Range of load versus deflection curves for unreinforced matrix and fiber reinforced concrete and fracture surface of SFRC [2]	11
Figure 2.2 Types of primal fiber.....	11
Figure 2.3 Corrosion from the side [4].....	16
Figure 2.4 Accelerated corrosion process.....	17
Figure 2.5 Crack patterns and internal crack types	19
Figure 2.6 State of the beam surfaces for the different series after a year of cyclic exposure to chloride solution [10]	21
Figure 2.7 Dumbbell specimen.....	22
Figure 2.8 Stress-strain curves	22
Figure 2.9 Direct tensile test [12].....	23
Figure 2.10 Stress-strain results for direct tensile tests [12]	23
Figure 2.11 Cross section of the tested beams [14].....	25
Figure 2.12 Load-deflection relationship of beams [14]	25
Figure 2.13 The stage of section RC beam loaded by bending to failure [15].....	27
Figure 2.14 Single fiber is intersecting the crack plane	29
Figure 2.15 Strain and stress distribution at cross section of steel fiber reinforced concrete beam at failure:	29
Figure 2.16 Modified stress distribution block [14].....	30
Figure 3.1 Flow chart of experimental program.....	31
Figure 3.2 Aramid fibers.....	32
Figure 3.3 Single and twist fibers.....	33

Figure 3.4 Dumbbell specimen [Unit: mm].....	34
Figure 3.5 Direct tensile test.....	35
Figure 3.6 Dumbbell briquette	38
Figure 3.7 Stress-strain relationship of AFRM.....	38
Figure 3.8 Dimensions and reinforcement details of the beam test specimen	39
Figure 3.9 Corrosion test set up	40
Figure 3.10 Breaking tension zone	41
Figure 3.11 Soaking broken-beam	42
Figure 3.12 Repairing beam by AFRM and mortar product in the market.....	42
Figure 3.13 Experimental setup.....	44
Figure 4.1 Compressive strength	47
Figure 4.2 Splitting tensile strength.....	47
Figure 4.3 Mode failure of AFRC	50
Figure 4.4 Stress – displacement relationship.....	51
Figure 4.5 Stress – displacement curves of ARFC with different fiber length.....	51
Figure 4.6 Stress – displacement curves of ARFC with different fiber shape.....	52
Figure 4.7 Crack pattern and crack width of SB-AFM beam (unit: mm).....	54
Figure 4.8 Crack pattern and crack width of NRB beam at the bottom (unit: mm).....	55
Figure 4.9 Crack pattern and crack width of SB-MP beam at the bottom (unit: mm).....	55
Figure 4.10 Surface of corroded reinforced bars.....	55
Figure 4.11 Load-midspan deflection behaviour	57
Figure 4.12 Concrete crushing failure	57

Figure 4.13 Load-midspan deflection behaviour of BC beam	60
Figure 4.14 Load-midspan deflection behaviour of NRB beam	61
Figure 4.15 Load-midspan deflection behaviour of SB-AFM beam	61
Figure 4.16 Load-midspan deflection behaviour of SB-MP beam.....	62
Figure 4.17 Cracks pattern of BC beam.....	64
Figure 4.18 Cracks pattern of NRB beam	65
Figure 4.19 Cracks pattern of SB-MP beam	65
Figure 4.20 Cracks pattern of SB-AFM beam.....	66
Figure 4.21 Crack width of BC beam (mm).....	67
Figure 4.22 Crack width of NRB beam (mm).....	67
Figure 4.23 Crack width of SB-AFM beam (mm).....	68
Figure 4.24 Crack width of SB-MP beam (mm).....	68
Figure 4.25 Crack width from Pi-gauges at the middle bottom soffit of the beams (mm).....	69
Figure 5.1 Material model for single reinforced concrete design	71
Figure 5.2 Stress-strain distribution at ultimate state of conventional beams	73
Figure 5.3 Stress-strain distribution at ultimate state of strengthened beam by AFRM	73

LIST OF TABLES

Table 2-1 Strength to weight ratio of fiber [3].....	13
Table 2-2 Tensile strength of commercial fiber [3].....	14
Table 2-3 Properties about melt, oxidation, decomposition temperature of fiber [2].....	14
Table 3-1 Mix proportion of 1-m ³ PC (kg/m ³)......	33
Table 3-2 Mix proportion of 1-m ³ AFRC (kg/m ³).	33
Table 3-3 Geometry parameters of aramid fibers	34
Table 3-4 The mechanical properties of the reinforcing bars.....	36
Table 3-5 Mix proportion of 1-m ³ AFRM (kg/m ³).	37
Table 3-6 Details of beam specimens	39
Table 3-7 The total time and electric current for corrosion test.....	41
Table 4-1 Compressive strength and splitting strength results	46
Table 4-2 Direct tensile results	49
Table 4-3 Material properties of all the beams.....	58
Table 4-4 The test results of all the beams.....	58
Table 4-5 Comparison of load	58
Table 4-6 Comparison of deflection	59
Table 4-7 Displacement ductility.....	62
Table 5-1 Properties of material.....	72
Table 5-2 Comparison ultimate load of modelling and experimental results	75

Chapter 1

INTRODUCTION

1.1 General

Aromatic polyamides (Aramid) were first introduced in commercial application in early 1960s with meta-aramid fibers that includes fibers know under trade names like Conex (Japan, Netherland), Arawin (Korean), New Star (China), and Kermel (France), Kevlar (USA). They are use in aerospace, military application, marine, tooling and recreational products. The aramid fibers are also can be used in construction.



Figure 1.1 Products of aramid fibers [1]

Aramid fibers provide properties like low maintenance, durability, energy saving safety and light weight. They come up with many solutions of application areas and offer potential for different building and construction products such as strengthening of concrete structures (aramid fabrics), concrete reinforcement (FRP rods, short-cut fibers), masonry reinforcement (grid, geotextiles). However, the cost of aramid fiber is higher than glass, basalt and steel fibers making them less common in structural. Nowadays, these are used to repair in special position where corrosion resistance and injury avoidance are key requirement.

In many countries, there are thousands of highways, bridges, marine constructions that have deteriorated due to corrosion and require large expenditures to rehabilitation. Until now, there are many researches use the superior corrosion resistance of aramid fibers to repair the corrode structures. One of the methods, using

externally bonded fiber reinforced polymer (FRP). It is high strength/density relationship, uncomplicated and quick to set-up. FRP was not significantly affected by the mass or geometry of the structures. However, FRP was known as a material which high cost, low modulus of elasticity, lack of ductility, anisotropy, and creep rupture. Therefore, it is another way to add short-cut aramid fibers into concrete for strengthening concrete structures and protection of concrete against micro cracks.

This thesis will concentrate to investigate the mechanical behavior of concrete reinforced with aramid fibers, hereinafter called as aramid fiber reinforced concrete (AFRC). And, the ability in repairing of corroded reinforce concrete beam by AFRC.

1.2 Objectives of the research

Aramid fibers have applied in many fields which will be future material, but in construction, it has got the lack of relating standard and research. Consequently, the purposes of this thesis will be additional for aramid fiber reinforced concrete standard and any later studies about aramid fibers. Furthermore, the superior properties was taken in order to apply in construction field. Therefore, the three main purposes of this thesis are:

- To investigate the effect of the presence of fibers and fiber geometry on the mechanical properties of aramid fiber reinforced concrete
- To investigate the flexural behaviour of corroded reinforced concrete beams which were repaired by aramid fiber reinforced mortar and mortar product available in the market.
- To propose the model for predicting the flexural capacity of RC beam, corroded RC beams, corroded beams repairing by aramid fiber mortar and mortar product in the market.

1.3 Scopes of the thesis

This research consists of scopes as follow:

- (1) Tensile behavior is based on the direct tensile test.
- (2) The accelerated corrosion test is used to induce corrosion in RC beams.
- (3) Repairing material is aramid fiber reinforced mortar and mortar product available in the market.
- (4) Flexural behaviour of reinforced concrete beam, corroded reinforced concrete beam, and reinforced concrete beams after repairing is studied.
- (5) Effects of creep and shrinkage are excluded in this study.

1.4 Thesis outline

This thesis is organized into six chapters.

Chapter 1 performs the basic knowledge, background, objectives, scopes, and thesis outline.

Chapter 2 provides the literature review. This part consists of six sections, there are mechanical properties of fiber reinforced concrete, and mechanical properties of synthetic fiber reinforced, and aramid fiber. Moreover, for the third section, there is general definition about accelerate corrosion and effect of corrosion on reinforced concrete beam. For fourth section, there are listed some papers about tensile mechanical of fiber reinforced concrete and mechanical properties of aramid fiber reinforced concrete. For fifth section, repairing corroded beam by mortar patch was observed. The modeling was assumed in sixth section.

Chapter 3 provides the experimental program of entire process. There were observed material, specimens, and test set-up of process.

Chapter 4 introduces the result of compressive, splitting, and direct tensile test of aramid fiber reinforced concrete. The results of corrosion of beams are also summarized in this chapter. The result of four-point bending test as will be shown by load-deflection relationship, crack pattern, width cracks and displacement ductility

ratio. Therefore, the result will perform the flexural behaviour of all of beams. Moreover, there will perform the presence of aramid fiber mortar on the flexural behaviour of beam.

In **Chapter 5**, the ultimate flexural capacity of beams was suggested by the prediction model. The results from modelling will compare with result from experiment.

The conclusion of this experimental study is given with the recommendations for future works in this **Chapter 6**.

Outline of thesis is shown detail in **Fig. 1.2**.



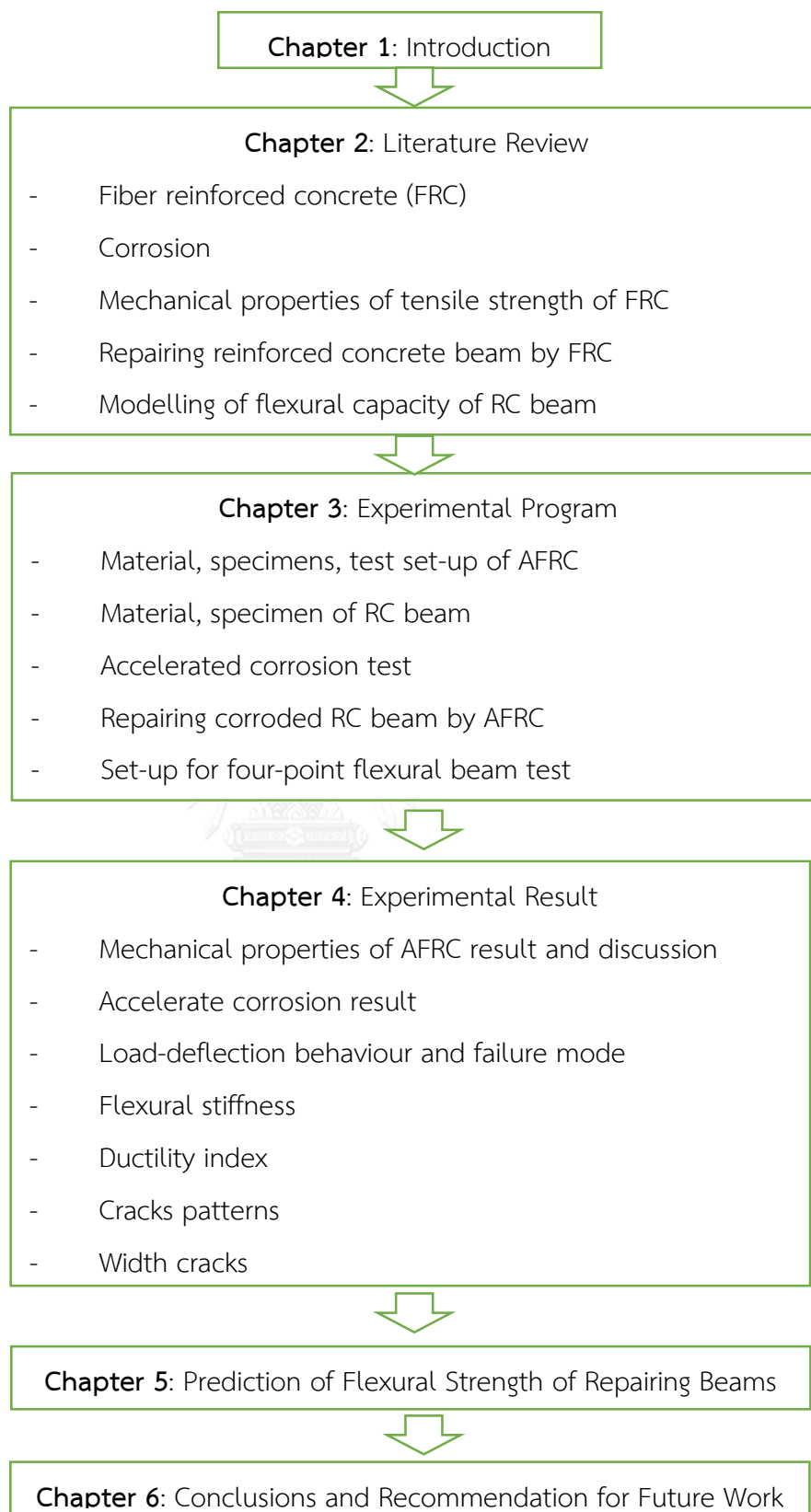


Figure 1.2 Outline of thesis

Chapter 2

LITERATURE REVIEW

2.1 Fiber Reinforced Concrete (FRC)

Fiber reinforced concrete (FRC) is concrete consisting of fibers material which increases its structural integrity. It contains short discrete fibers that are uniformly distributed and randomly oriented. Fibers include glass fibers, steel fibers, natural fibers and synthetic fibers. Each type of fiber lend varying properties to the concrete. In addition, the character of fiber reinforced concrete changes with varying fiber materials, concretes, orientation, geometries, densities, and distribution.

Concrete is relatively brittle, and its tensile strength is typically only about one tenths of its compressive strength. Therefore, fibers have been used to reinforce brittle materials. Their main purpose is to increase the energy absorption capacity and toughness of the material. In addition, fiber also increases tensile strength and flexural strength of concrete structures. Since ancient time, straw was used to reinforce sun baked bricks, and horse hair was used to mortar and plaster. A pueblo house was built around 1540, was known as the oldest house in the U.S., is constructed of sun baked adobe reinforced with straw. In 1898, Hatschek invested cement paste matrix which was used to asbestos fiber. Asbestos cement construction products are widely used until the world today. In modern times, a large range of materials science incorporate fibers to enhance properties of composite. The enhanced physical properties include compressive strength, tensile strength, crack resistance, elastic modulus, crack control, fatigue life, resistance of impact and abrasion, durability, fire resistance, expansion, shrinkage, and thermal characteristics.

Related with tensile strength and strain capacity in fracture, unreinforced concrete has low value. These have disadvantage in structure, then, it necessary optimization of structure performance is needed. In concrete matrix, fibers are discontinuous and are distributed randomly. With conventional reinforcement, fibers are used in concrete structural applications.

Fabrication of fiber is flexibility, therefore, fiber reinforced concrete is economic and useful construction material. In U.S. and Europe, precast glass fiber reinforced concrete architectural cladding panels are economically viable. Steel and synthetic fiber reinforced concrete was used in lieu of welded wire fabric reinforcement in slabs on grade, mining, tunneling, and excavation support applications. In addition, the range of load versus deflection curves for unreinforced matrix and fiber reinforced concrete are shown at **Fig 2.1**. These shown that with the presence of fiber, concrete still resisted the load after getting the peak load.

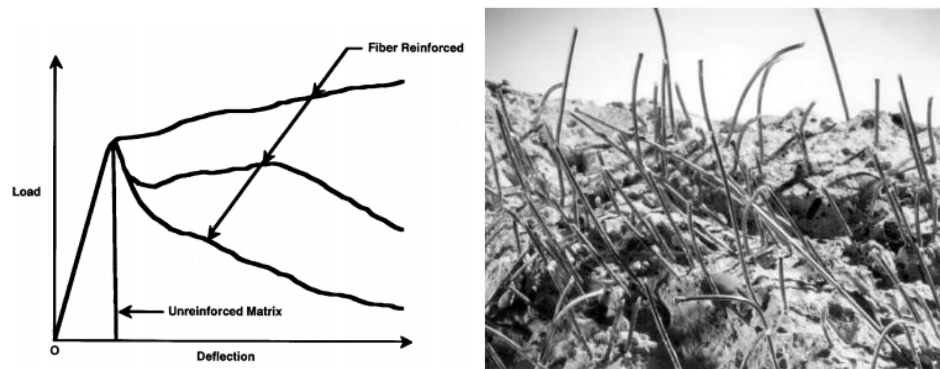


Figure 2.1 Range of load versus deflection curves for unreinforced matrix and fiber reinforced concrete and fracture surface of SFRC [2]

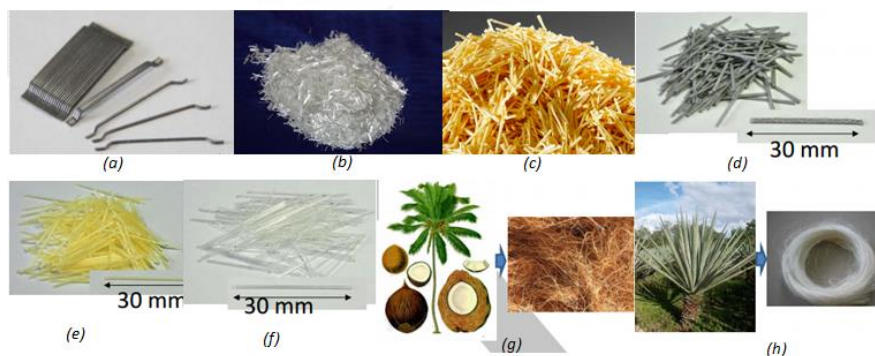


Figure 2.2 Types of primal fiber

- (a) Steel fibers (b) Glass fibers (c) Aramid fibers (d) Polypropylene (PP)
 (e) Polyvinyl alcohol (PVA) (f) Polyethylene terephthalate (PET)
 (g) Coconut (h) Sisal

For commercial and experimental, numerous fibers types available was used. The primary fiber categories are steel, glass, synthetics (acrylic, aramid, nylon, polyester, polyethylene (PE), polypropylene (PP), poly vinyl alcohol (PVA), and natural fiber material (coconut, sisal, bamboo, sugarcane bagasse, and jute, wood). Some type of fibers is shown in **Fig 2.2**.

2.2 Synthetic fiber

Synthetic fibers are a man-made fibers. These were researched and developed in the petrochemical and textile industries. Synthetic fibers derived from organic polymer. Fiber types were carried out to mix in Portland cement concrete, were consisted of: acrylic, aramid, carbon, nylon, polyester, polyethylene and polypropylene. The polymer made of crystalline portion, then, these were converted on heating from a solid to a glassy or liquid state. At that time, synthetic fiber are said to be melted. In addition, oxidation is a typical cause of decomposition of synthetic fiber. The chemical reaction of fiber and oxygen is cause of oxidation. Decomposition is necessary to mention because fiber will change color, fume, and change significantly chemical structure.

In 1965, synthetic fiber was reported as a component of construction materials. For U.S. Army Corps of Engineers Research and Development Section, synthetic fiber was used in blast resistant structures. Synthetic fiber, steel fiber, and glass fiber were carried with similar of length and shape. There were 13 to 25 mm in length and the length to diameter ratio around 50 to 100. The result of this project shown that with addition a small quantities, 0.5 percent of volume, of synthetic fiber to concrete, the composite material can increase both ductility and resistance load.

With a necessary application in new area, higher fiber contents were considered in many research which mention about toughness index and other factor. After first crack, the load carrying capacity depend on the toughness of fiber and concrete matrix.

2.3 Aramid fibers

Aramid fiber was said as aromatic polyamide fiber. There is material made from polymeric material which has high value of modulus. Aramid fiber was first discovered in 1965. After many years of experimental research, a method to produce that material in fibers form was finally developed. Aramid fibers were initially produced for commercial applications by the early 1970s. Some commercial application as ballistic protection products, hard ballistics, soft body armour, helmets, civil engineering products, composites, cut-protection products, elastomer reinforcements, engineering plastics, friction products, heat-protection products, optical fiber cables, reinforced pipes, ropes and cables, sealing materials, specialty paper, tires. Attempts to incorporate this fiber into concrete as a form of reinforcement began by the late 1970s. In civil engineering product consist of strengthening of structures (aramid fabrics), concrete reinforcement (FRP rods, short-cut fibers), masonry reinforcement (grid, geotextiles).

Comparison properties between aramid fiber and other fibers is shown in table below:

Table 2-1 Strength to weight ratio of fiber [3]

Material	Strength to weight	Ultimate strength	Density
	kN.m/kg	MPa	g/cm ³
Kevlar (Aramid)	2514	2757	1.44
Carbon fiber	2457	4137	1.75
Carbon laminate	785	1600	1.5
E Glass fiber	1307	3450	2.57
E Glass laminate	775	1500	1.97
Polypropylene	89	19.7-80	0.91
Steel alloy ASTM A36	254	400	7.8
Nylon	69	75	1.15

Aramid fibers yarns have many properties as follow: high tensile strength, high stiffness, low density, low creep (when compared with other synthetic fibers such as nylon or polyester), stress rupture, impact and shock loading resistance, chemical and environmental resistance, resistance from high temperature, electrical non-conductivity [3].

Aramid fibers have remarkable strength to weight ratio when compared to other commercial fibers.

This below table is illustrated in tensile strength of aramid fiber and other commercial fiber. Therefore, aramid fiber has a great number of variables.

Table 2-2 Tensile strength of commercial fiber [3]

Material	MPa units
Carbon steel 1090	650
Stainless steel AISI 302	860
Polypropylene	19.7-80
E Glass in a laminate	1500
Carbon fiber in a laminate	1600
Kevlar (aramid)	2757

Table 2-3 Properties about melt, oxidation, decomposition temperature of fiber [2]

Material	Melt, oxidation, or decomposition temperature, F
Aramid	900
Carbon	752
Nylon	392-430
Polyethylene	273
Polyester	495

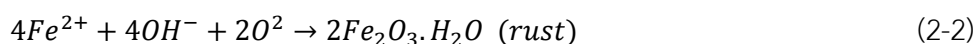
Aramid fiber could have complicated conditions. Therefore, the application of aramid fiber in construction is a great solution in the future.

2.4 Corrosion

2.4.1 General

Corrosion of the steel reinforcement is typically a cause of deterioration of concrete structure. The problem of corrosion has received world-wide attention. Recently, the number of corroded reinforced concrete structures is increasing. Corrosion damage of reinforced concrete is a serious problem that needs to be addressed. This damage is a large drain on the economy. Such corroded structures have to be repaired to keep safety, usability and appearance of the structure. Various types of repairing methods are applied to such corroded structures. However, there are few studies on repaired RC structures using fiber-reinforced concrete.

When corrosion happens, oxygen reaches the surface of steel by passing through the cement matrix. Then, it reacts with some ions such as chlorides to destroy the protective film on the steel surface. Further, more contaminants can react with steel, like making the condition become acidic. This acidic condition causes the protective film on the steel to start corroding. Finally, this oxidation process results in the segregation of steel and the amount of water. The chemical reaction can be explained with two processes as follows:



The corrosion product is rust, which occupies a larger volume than the reinforcement, then, leads to cracking and spalling of the concrete. Iron (III) oxide trihydrate, $Fe_2O_3 \cdot 3H_2O$, common red rust, occupies a volume a little over six times that of the steel that corroded. Depending on the depth and spacing of the reinforcing bar, these cracks may form perpendicular to the concrete surface and immediately above the corroding bar or the crack may form parallel to the surface of the concrete and at the level of the bar.

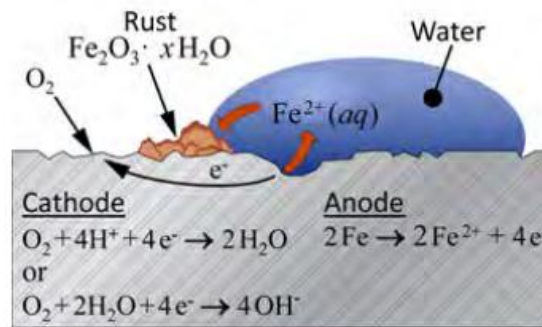


Figure 2.3 Corrosion from the side [4]

2.4.2 Accelerated corrosion

Corrosion of reinforcement is a process occurring in a long time in concrete structure. Concrete has the self-protective nature, therefore, it needs a long time to initiate and progress of reinforcement corrosion, even though in the situation of extremely corroded exposure condition. It is hard to reach a meaningful degree of reinforced corrosion in a limited duration for research studies which evaluate the loss of bonding and loss of load capacity of corroded reinforcement of concrete structure. Therefore, many researchers used accelerated corrosion as a technique for corroded reinforcement. In the recent time, accelerated corrosion of reinforcement in concrete structure was used in artificial climate environment country. Due to the similarity of the surface characteristic of the corroded reinforcement under natural and by accelerated corrosion, it is becoming important to assess the durability of reinforced concrete structure.

The electrochemical way was induced in accelerated corrosion test. It matches the display of the specimens on aggressive solution with the electric current for simulating the chlorides migration. The specimens were immersed in an aqueous solution of 3 percent of NaCl. The detail of direct current supply was used for the accelerated corrosion process for the beam specimen as shown in **Fig. 2.4** [5].

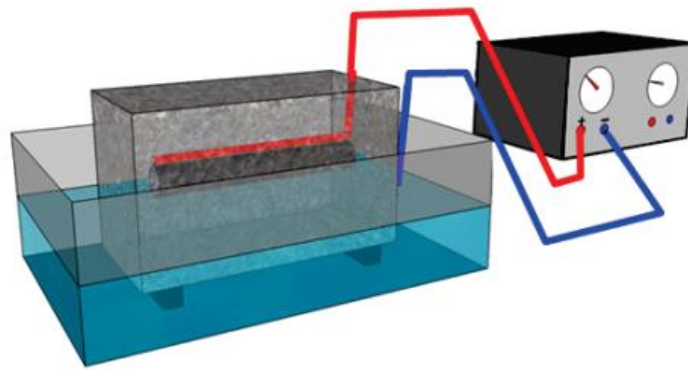


Figure 2.4 Accelerated corrosion process

2.4.3 The effect of corrosion on RC beams

Corrosion of steel reinforcement reduced the load carrying capacity of RC beams. The reduction in the beam strength was almost proportional to the reduction in the steel cross sectional area due to corrosion. The presence of flexural cracks due to sustained load slightly increased the reduction in the steel mass loss and hence the reduction in the beam strength. Study by Tamer et al. [6] is shown that for levels of corrosion less than approximately 15% steel mass loss, the deflection at failure increased due to corrosion that reduced the area of the tensile steel reinforcement. At higher levels of corrosion, when pitting corrosion occurred, the deflection at failure of the beam decreased. Pitting corrosion had a small effect on decreasing the deflection capacity when the beams were corroded under a sustained load.

According to Lamya Amleh and Saeed Mirza et al. [7], the research are shown that the bond strength at the steel-concrete interface decreases rapidly with an increase in the corrosion level, especially in the case of any severe localized corrosion. The bond behaviour is influenced by the deterioration of the reinforcing bar ribs and by the reduced adhesion and cohesion at the longitudinal splitting cracks resulting from corrosion. In the tension tests simulating severe localized corrosion, the bond strength and the number of transverse cracks decreases as the level of corrosion increases until it becomes negligible; for example, a 4 percent loss of weight due to corrosion, accompanied by transverse cracks, resulted in a 9 percent loss of bond

strength, while a 17.5 percent weight loss, with no transverse cracks before yielding of the bar, resulted in 92 percent loss of bond between the steel and the surrounding concrete. Corrosion, especially when severely localized, causes a significant reduction of the interlocking forces between the ribs and the concrete keys due to the deterioration the primary mechanism of the bond in deformed bars, which is the transfer of forces by mechanical interlocking of the ribs, and hence, the bond strength decrease significantly. The associated decrease in the tension stiffening with an increase in the corrosion level signifies the initiation of bond breakdown, which is very much influenced by the surface conditions of the bar and the level of its adhesion and cohesion to the surrounding concrete.

For most damaged or deteriorated concrete structure, there has a number of options to decide the repair and protection solution to reach the future requirement of the concrete structure. The options consist of: (1) do not repair, (2) deteriorate the RC structure or its load capacity, (3) resistance or reducing more damage without repairing, (4) improvement or strengthening all or part of the RC structure, (5) annihilation. For improving strengthening of RC structure, numerous methods were applying consist of using externally bonded carbon fiber reinforced polymer (CFRP), grass fiber reinforced polymer (GFRP), textile reinforced concrete (TRC), jacket with fiber reinforced concrete and external post-tensioning. The following researches are some examples of the application fibers (or composite) in repairing reinforced concreted beams and some special structures.

2.4.3.1 Bond strength

Study by Jin Wei-Liang et al. [8] on how effect of corrosion on bond behaviour suggested that the bond strength between deformed bars and concrete at first increased a little with the increasing corrosion. This also can be explained on the basis of the surface roughness of steel bars. Then the bond strength declined consistently because of the reduction in the profile of the bar fibs. Cracking seemed to have no effect on the bond strength between deformed bars and concrete.

Lamya Amleh et al. [7] shown how corrosion influence on bond between reinforcement and concrete. The study dedicated that with increasing the corrosion level, the bond strength at the reinforcement-concrete interface decreases rapidly, especially in the case of extremely localized corrosion. The deterioration of the reinforcing bar ribs and reducing adhesion, and reducing cohesion at the reinforcing bar surface influenced bond behaviour. Resulting of corrosion is widening of the longitudinal splitting cracks. The tension tests simulated severe localized corrosion, as the corrosion level increases, then, leading to decreases the bond strength and number of transverse cracks; for example, mass loss by 4 percent due to corrosion, resulted in accompanied by transverse cracks, and resulted in a 9 percent loss of bond strength, while mass loss by 17.5 percent, resulted with no transverse cracks before yielding of the bar, and resulted in 92 percent loss of bond between the reinforcement and the surrounding concrete. The corrosion level increases lead to the width of transverse cracks increase. Therefore, it reduced significantly bond strength between the reinforced steel bar and the concrete.

2.4.3.2 Corrosion crack patterns and widths

Figure 2.5 indicates the defined internal crack types shown in crack patterns. The study of H. Nakamura et al. [9] cracks due to rebar corrosion.

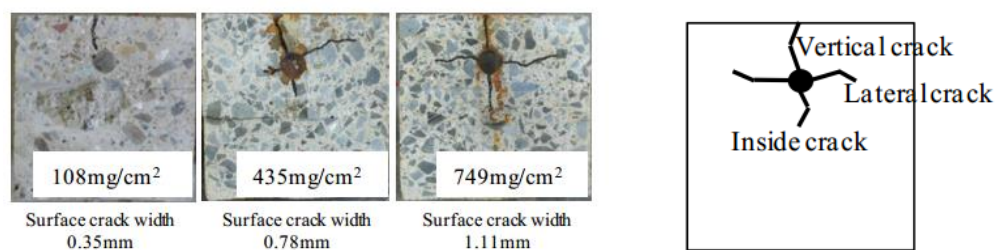


Figure 2.5 Crack patterns and internal crack types

Vertical crack occurred on the surface of concrete cover at the initiation of visible cracks. After level of corrosion increase, the propagation of crack lead to inside the concrete cover. Then, continue with lateral cracks and increasing their length. Moreover, rush of steel lead to crack at concrete from the rebar.

2.4.3.3 Flexural capacity

Tamer et al. [6] shown performance of corroded- damaged reinforced concrete beam. The study indicated that corrosion of steel reinforcement reduced the load capacity of RC beams. The reduction in the beam strength was almost proportional to the reduction in the steel cross sectional area due to corrosion. For the level of corrosion less than approximately 15% mass loss, the deflection capacity of the beam increased due to corrosion that reduced the area of tensile steel reinforcement. At higher levels of corrosion, when pitting corrosion occurred, the deflection capacity of the beam decrease.

2.4.4 The effects of corrosion on reinforced concrete with fibers addition

Development of crack can be resisted by fibers in either conventional concrete or fiber reinforcement concrete no matter with dosage. Thus, fiber gives advantageous in structure in term of limitation of crack. However, it still become questionable for steel fiber resistance in chloride environment. Therefore, Chalmers University of Technology [10] investigated the challenge application fiber reinforcement both in general and particular RC structure in relation with corrosion that induced by chloride. More, evaluating the effectiveness to resist crack by corrosion for fiber reinforcement in conventional reinforced concrete.

From that study, with the presence of steel fiber in concrete, steel fiber reinforced concrete increased resistance corrosion. It mean to decrease the chloride-induced corrosion when comparing with conventional reinforcement. The depth of cover concrete can be significantly reduced corrosion for concrete specimens. Furthermore, the study was inspected of the surface of many series of fiber reinforced concrete which consist of steel fiber, synthetic fiber, hybrid fiber, and plain concrete after a year of cyclic exposure. The study shown that the series of plain, steel fiber, hybrid fiber concrete isolated rust stains spotting on the surface of specimens. However, the series of the specimens was carried out by synthetic fiber which can resisted the spotting of rust stains in the surface of the specimens.



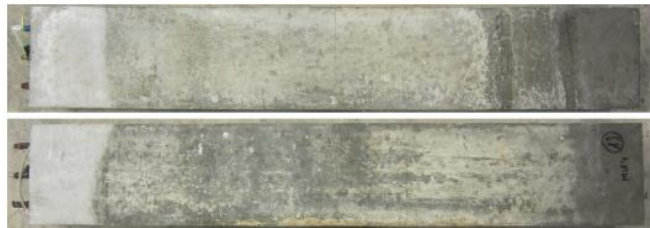
(a) Plain series



(b) Steel fiber series



(c) Hybrid fiber series



(d) Synthetic fiber series

Figure 2.6 State of the beam surfaces for the different series after a year of cyclic exposure to chloride solution [10]

2.5 Mechanical of fiber reinforced concrete

2.5.1 Tensile strength of fiber reinforced concrete

Yuan Haiyan et al. [11] was conducted tensile strength on steel fiber reinforced concrete. The direct tensile test was carried out through Universal Testing Machine with a self-designed test equipment as show in **Fig 2.7**.

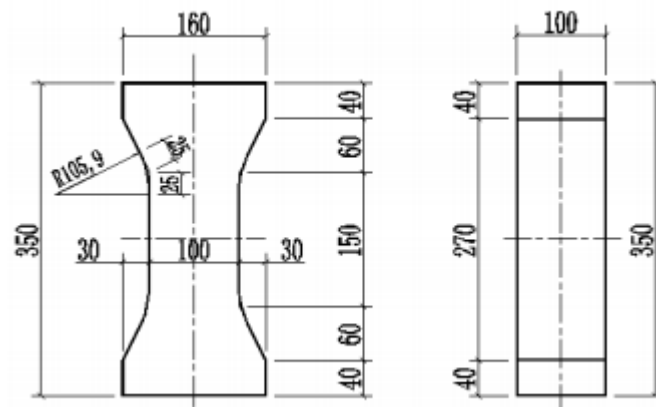


Figure 2.7 Dumbbell specimen

The tensile stress-strain curves obtained in the direct tensile tests are shown in **Fig. 2.8**. It can be seen that the curve interrupted on the peak point similar as normal concrete when $V = 0\%$. When the steel fiber content by volume V increased, the curve decreased slowly after the maximum load. The descending portion of the curve of $V = 2\%$ was more flat than $V = 1\%$ because there is more steel fiber absorbing energy in the specimen.

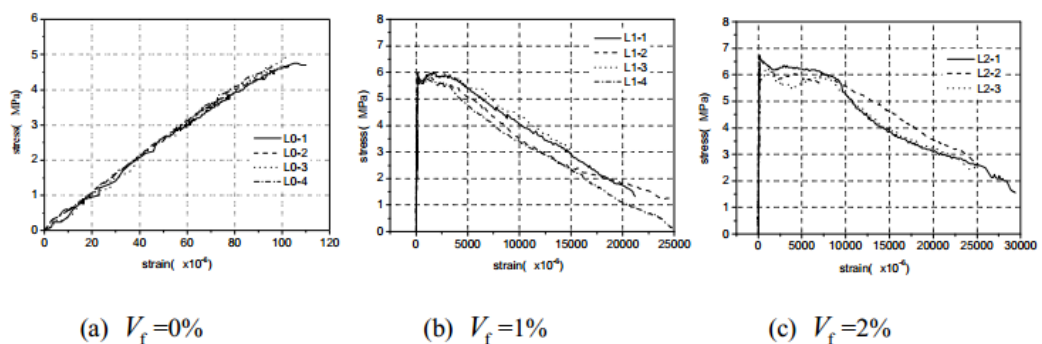


Figure 2.8 Stress-strain curves

A.P. Lampropoulos et al. [12] indicated the tensile strength of ultra-high performance fiber reinforced concrete (UHPFRC). Direct tensile tests of six dumbbell specimens were carried out. The experimental results indicated variation of the tensile strength between 11.74 MPa and 14.20 MPa. Digital Image Correlation (DIC) system was used during the testing in order to monitor the crack opening and the strain distribution at the moment when the first crack appeared. **Figure 2.9** shown the dimension of specimen and experimental set-up.

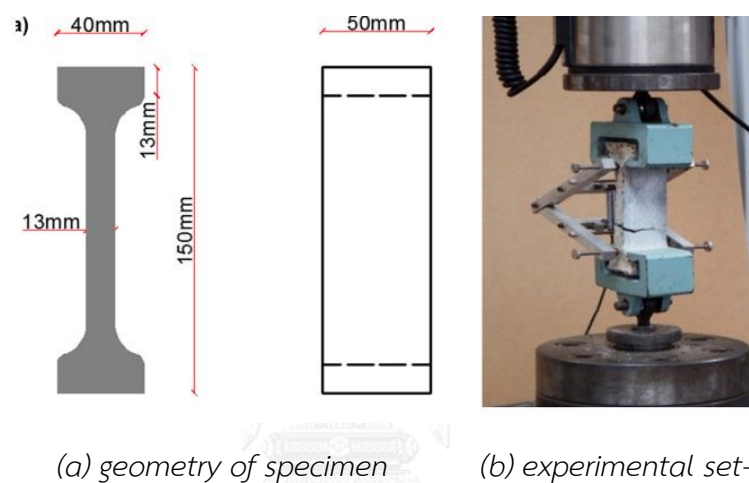


Figure 2.9 Direct tensile test [12]

According to the results as shown in Fig. 2.10, the strain is uniformly distributed along the specimen in the elastic part of the stress-strain distribution (strain below 0.001).

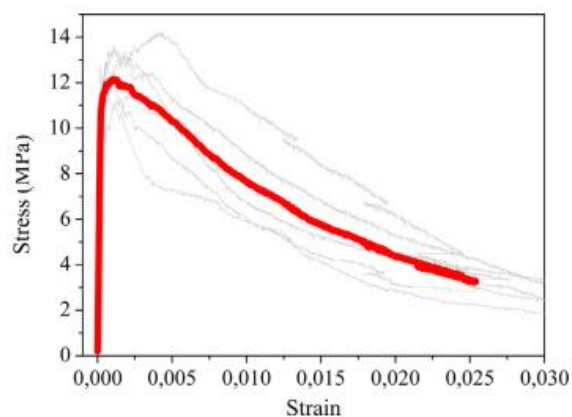


Figure 2.10 Stress-strain results for direct tensile tests [12]

At the strain from 0.002 to 0.005, many micro cracks was opened into specimens. The cracking opening for strain has value higher than 0.005, all specimens was extended.

2.5.2 Ultra high strength fiber reinforced concrete using aramid fiber

Previous study conducted by Y. Uchida and T. Takeyama [13] focusing high strength and elastic modulus that aramid fibers have compared other fibers in term of substitution of steel fibers. Then, investigation of mechanical properties from UHFRC using aramid fibers is conducted using different sizes and shape of aramid fiber in term of compressive strength and post-cracking strength in notched beam is also inspected.

This is using water binder ratio 0.19 with varies of diameter, length, and shapes of aramid fibers, then, compared those with steel fiber performance. Varies of aramid fibers used: Type I: diameter 12 μ m, length 12 mm; Type II: 45 μ m, and 3, 6, 8, and 12mm for diameter and length respectively; Type III: vinyl ester resin bundled into stick with 267 fibers has 0.2 mm 12 mm for diameter and length, sequently. Lastly, steel fiber 0.2 mm and 15 mm for diameter and length respectively.

Assuming a target flow value of 200 mm in consideration of the ease of placing, the maximum fiber content is determined for each type of aramid fiber. Base the results, the maximum fiber contents were determined. Fiber contents of 1.0%, 3.0%, 2.0%, 1.25%, 1.0%, and 1.75% were selected for 12 μ -6mm, 3mm, 6mm, 8mm, 12mm, and 12mm-B respectively. A fiber content of 2.0% is adopted for steel fibers for reference without investigating the accommodated maximum.

Specimens with aramid fiber cured in hot water is compared with different length of fiber which are 3, 6, 8 mm. Those are achieved compressive strength around 220 Mpa. In contrary, for fiber 12 mm length and bundle fiber have less which are 180 to 190 Mpa. In addition, specimens with steel fiber has highest compressive strength among other around 240 Mpa or 10% higher.

2.6 Repairing reinforced beam by fibers reinforced concrete

To improve bending moment capacity of RC beams, Shahid Iqbal et al. [14] applied steel fiber reinforced high strength light-weight self-compacting concrete (SHLSCC). Eight beams were carried out. One beam was conducted as the reference beam which without strengthening and using normal vibrated concrete (NVC). One beam with lower half as SHLSCC and upper half as NVC. Six beams were carried out with using NVC similarly with reference beam. Then, two beams were repaired by the jacket. Four beams were repaired by layer at the tension zone.

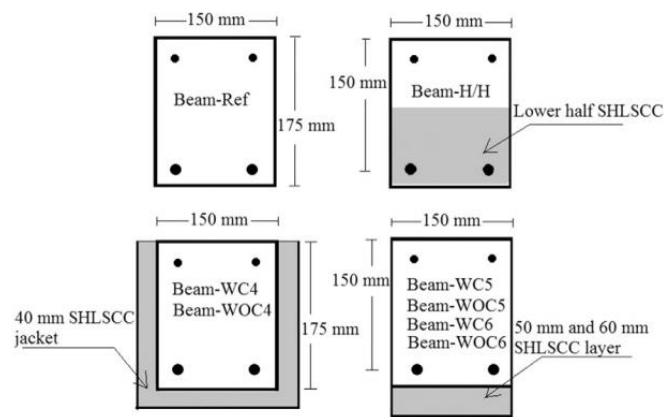


Figure 2.11 Cross section of the tested beams [14]

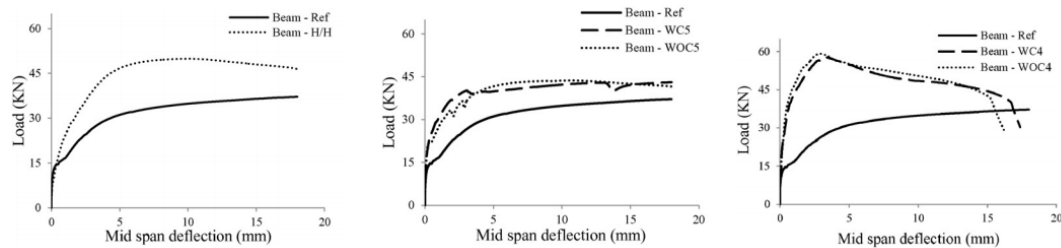


Figure 2.12 Load-deflection relationship of beams [14]

According to the results as shown in Fig. 2.12, there are significant improvement in stiffness of strengthened beams. Moreover, there are improvement by 14-58% at the peak load with the beams repairing by 40 mm, 50 mm, and 60 mm at the tension zone of SHLSCC layer. The beams repairing as a jacket increased by 31% at the peak load.

2.7 Modelling of flexural capacity of RC beams

Figure. 2.11 describes the behavior of a reinforced concrete beam, which loaded by two concentrated forces. Loads are placed symmetrically through the beam axis. Principal stress trajectory indicates that, in pure bending area, the principal stress running parallel to the beam axis. Cross section consists of tensile and compressive stress. Area flexural and shear simultaneously, principal stress inclined with beam axis. In areas near point loads, principal stress trajectories change direction very large and often called the disturbance area.

Stage 1: Tensile stress is less than tensile strength of RC beam, which has not appeared cracks.

Stage 2: When the concrete tensile stress reaches tensile strength, the first cracks will appear. Due to tensile stresses of this beam parallel to the axis lead to flexural cracking perpendicular to the axis direction. The increase load lead to cracking in shear zones. Initially, these cracks have perpendicular direction to the beam axis. However, with the developing the height of beam, they change slope very fast and become inclined cracks. The cracks are called flexure-shear cracks. After cracks are appeared, if the beam designed reasonable, the tensile reinforcement and concrete in compressive region still work in elastic limit.

Stage 3: If the load continues to increase, the cracks will continue to grow, especially the incline. Some small cracks will incorporate into large cracks at between of the height beam. Observed deflections are very large corresponding to the reduction of beam stiffness. At this time, the beam is nearly destructive stage. At the D-D section, strain is observed still elastic. However, for C-C section, strain is observed nonelastic.

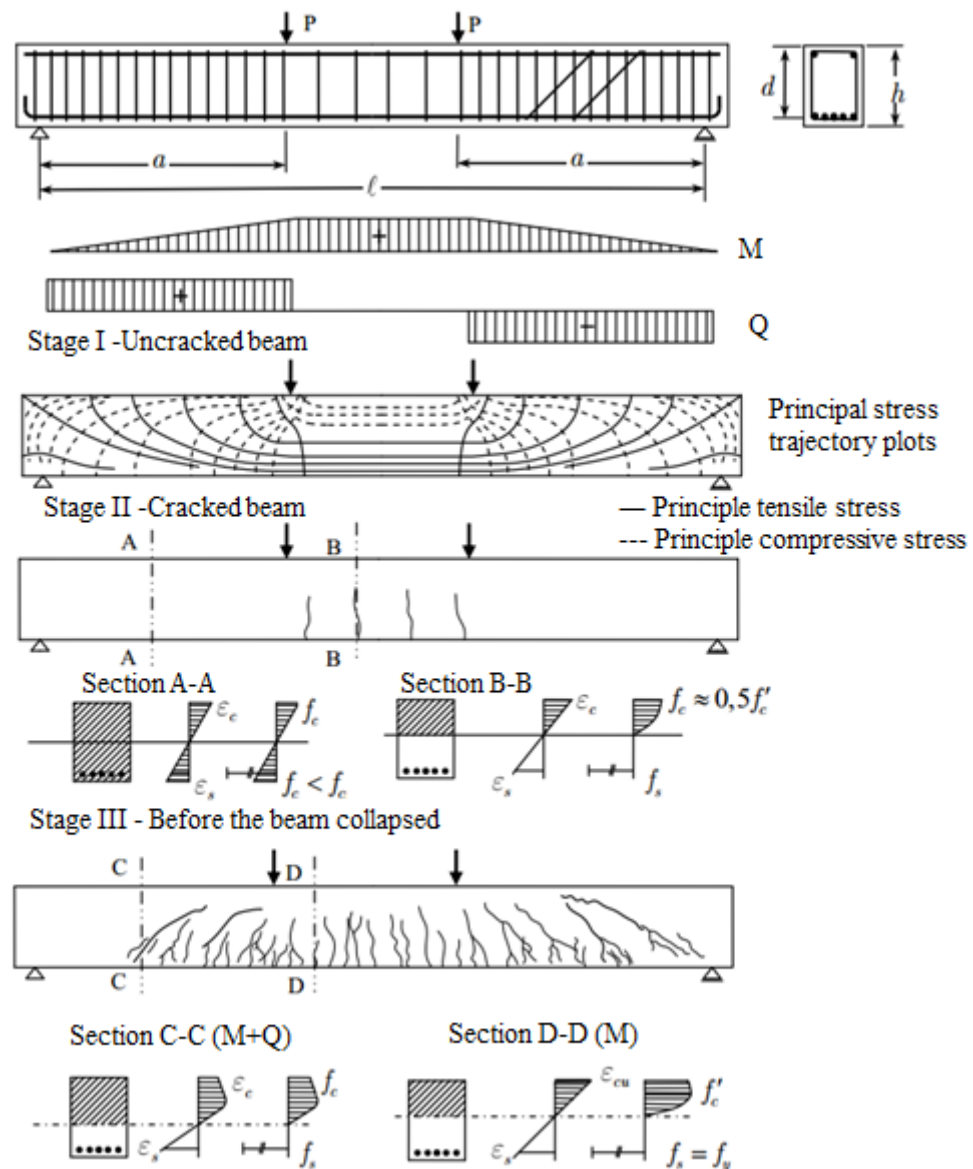


Figure 2.13 The stage of section RC beam loaded by bending to failure [15]

Xiliang Ning et al. [16] shown a method incorporating fiber contribution to the post-cracking tensile strength of concrete in the flexural analysis of steel fiber reinforced self-consolidating concrete (SFRSCC) beam is also suggested. The method is shown as follows.

Stress-strain relationship of materials:

A Hognestad stress-strain relationship was used for concrete in compression:

$$\sigma_c = \begin{cases} f'_c \left[1 - \left(1 - \frac{\epsilon_c}{\epsilon_o} \right)^2 \right] & (for) 0 < \epsilon_c \leq \epsilon_o \\ f'_c \left(1 - 0.15 \frac{\epsilon_c - \epsilon_o}{\epsilon_{cu} - \epsilon_o} \right) & (for) \epsilon_o < \epsilon_c \leq \epsilon_{cu} \end{cases} \quad (2-3)$$

Where:

f'_c is the compressive strength of concrete; ϵ_o is the strain at peak stress of concrete, taken as 0.002; and ϵ_{cu} is the ultimate strain of concrete, taken as 0.003 for plain concrete and 0.0035 for steel fiber reinforced concrete.

The stress–strain relation of longitudinal reinforcement used in the study is expressed as:

$$\sigma_s = \begin{cases} E_s \epsilon_s & (for) 0 < \epsilon_s \leq \epsilon_y \\ f_y + \frac{f_{tu} - f_y}{\epsilon_{tu} - \epsilon_y} \epsilon_s & (for) \epsilon_y < \epsilon_s \leq \epsilon_{tu} \end{cases} \quad (2-4)$$

Where:

E_s is the elastic modulus of reinforcement; f_y, f_{tu} are the yielding and ultimate strength of reinforcement in tension, respectively; ϵ_y is the yielding strain of reinforcement and is calculated as $\epsilon_y = f_y/E_s$; and ϵ_{tu} is ultimate tensile strain of reinforcement, taken as 2.5% according to RILEM [17].

The stress transfer capability of steel fiber perpendicular to crack is expressed as:

$$\sigma_{fu} = \frac{1}{3} \alpha \tau_f V_f (1 + f) \quad (2-5)$$

Where:

α is the aspect ratio ($\alpha = l_f/d_f$, l_f and d_f are the length and diameter of fibers, respectively); τ_f is the average fiber matrix interfacial bond stress; V_f the volume fraction of fibers; f is the coefficient of friction between concrete and fiber sheared over the crack edge, taken as 1/3 recommended by Stroeven [18].

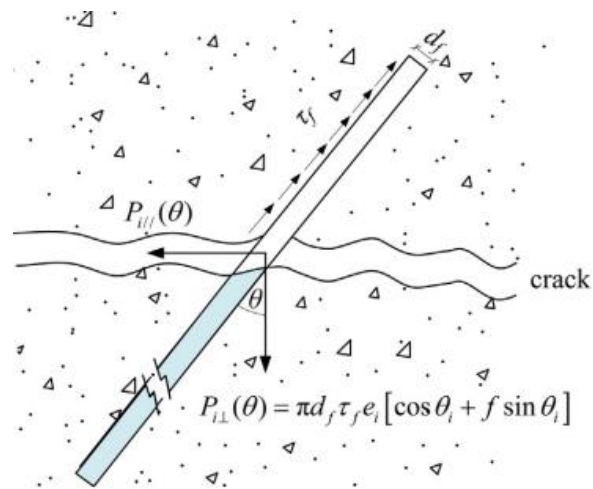


Figure 2.14 Single fiber is intersecting the crack plane

Based on the plane section assumption, then:

$$\varepsilon_k = \Phi_i \left(c - k\Delta h + \frac{\Delta h}{2} \right)$$

$$\varepsilon_s = \Phi_i (d - c)$$

$$\varepsilon_{ct} = \Phi_i (h - c)$$

(2-6)

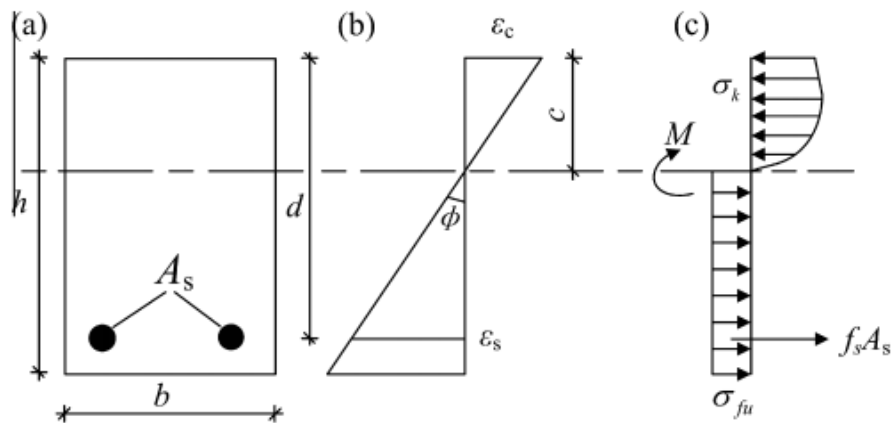


Figure 2.15 Strain and stress distribution at cross section of steel fiber reinforced concrete beam at failure:

(a) cross-section; (b) strain distribution; (c) stress and force distribution

The equilibrium condition of force and moment for the selected beam section results in:

$$P = \sum_{k=1}^m \sigma_k(\varepsilon) b \Delta h - f_s A_s - \sigma_{fu} b (h - c)$$

$$M = \sum_{k=1}^m \sigma_k(\varepsilon) b \Delta h \left(\frac{h}{2} - k \Delta h + \frac{\Delta h}{2} \right) + f_s A_s x (d - c) + \sigma_{fu} b (h - c) \left(\frac{h - c}{2} \right) \quad (2-7)$$

During fiber was pulled out, the bonding between the fibers, friction forces, and the surrounding matrix was acting. Therefore, the initiation and propagation of cracks were resisted by fibers. The model of steel fiber reinforced high strength light-weight self-compacting concrete (SHLSCC) was suggested by Shahid Iqbal et al. [14]. The detail suggested model is show in **Fig. 2.16**.

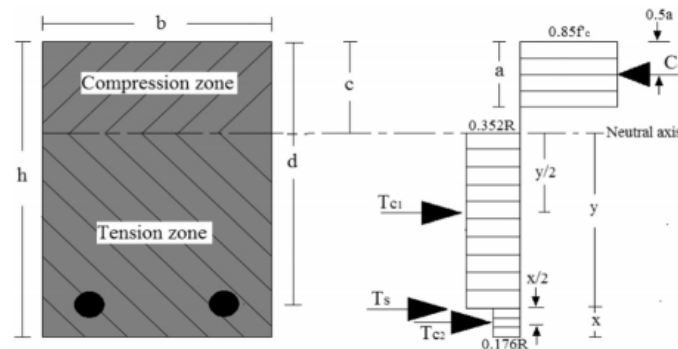


Figure 2.16 Modified stress distribution block [14]

In **Fig. 2.16**, T_{c1} is the tensile force in concrete in tension zone above longitudinal steel rebar, T_{c2} is the tensile force in concrete in tension zone below longitudinal steel rebar, T_s is the tensile force in longitudinal steel rebar in tension zone. The results from experimental was compared with the result from the model. The comparison showed maximum variation 4%. The prediction moment capacity calculating from stress distribution model is effectively when applying for strengthened beams.

Chapter 3

EXPERIMENTAL PROGRAM

3.1 General

Experimental program consists of two stage:

Stage 1: Study on mechanical properties of aramid fiber reinforced concrete (AFRC). In this stage, three test were carried out: compressive test, splitting test and direct tensile test. The proper fibers length and shape was selected based on the experimental result in Stage 1. The proper fibers length and shape was 40-mm long and twist fibers. Therefore, fibers with 40 mm long, and twisted shape have been material in aramid fibers reinforced mortar (AFRM) which material were used to strengthen corroded reinforced beams (stage 2).

Stage 2: Four beams were carried out with dimension as 150x200x1400 mm. Three beams were conducted accelerated corrosion to approach 10% mass loss. Two beams were broken at the tension zone. Shortly afterward, aramid fibers reinforced mortar (AFRM) and mortar product available in market used to repair broken-beam. After curing 14 days, four beams were conducted four-point flexural test.

The diagram of entire test is shown in **Fig. 3.1**.

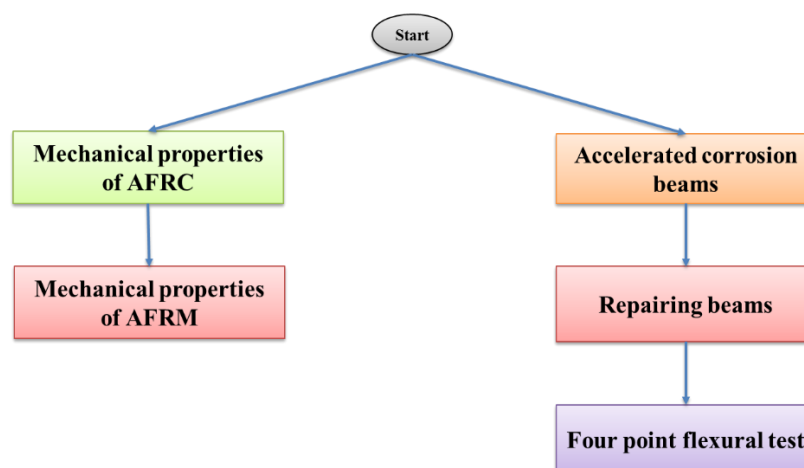


Figure 3.1 Flow chart of experimental program

3.2 Mechanical properties of aramid fibers reinforced concrete

3.2.1 Material and mix-design

The mixture was designed to provide a cylindrical compressive strength of 30 MPa after 7 days. Two proportions were used. **Table 3-1** and **Table 3-2** show the proportion for plain concrete (PC) and AFRC, respectively. Water to binder (cement and fly ash) ratio has been set to 0.48. The aggregates added to the mixtures were sharp edge type. Coarse aggregate, sand, ordinary Portland cement (OPC) and super plasticizer (Type: Master Glenium ACE 8320) has been used. Super plasticizer was added with 0.3% of binder weight for plain concrete. Since aramid fibers absorbed some water, super plasticizer was added with 0.85% of binder weight to provide adequate workability of the mixtures.

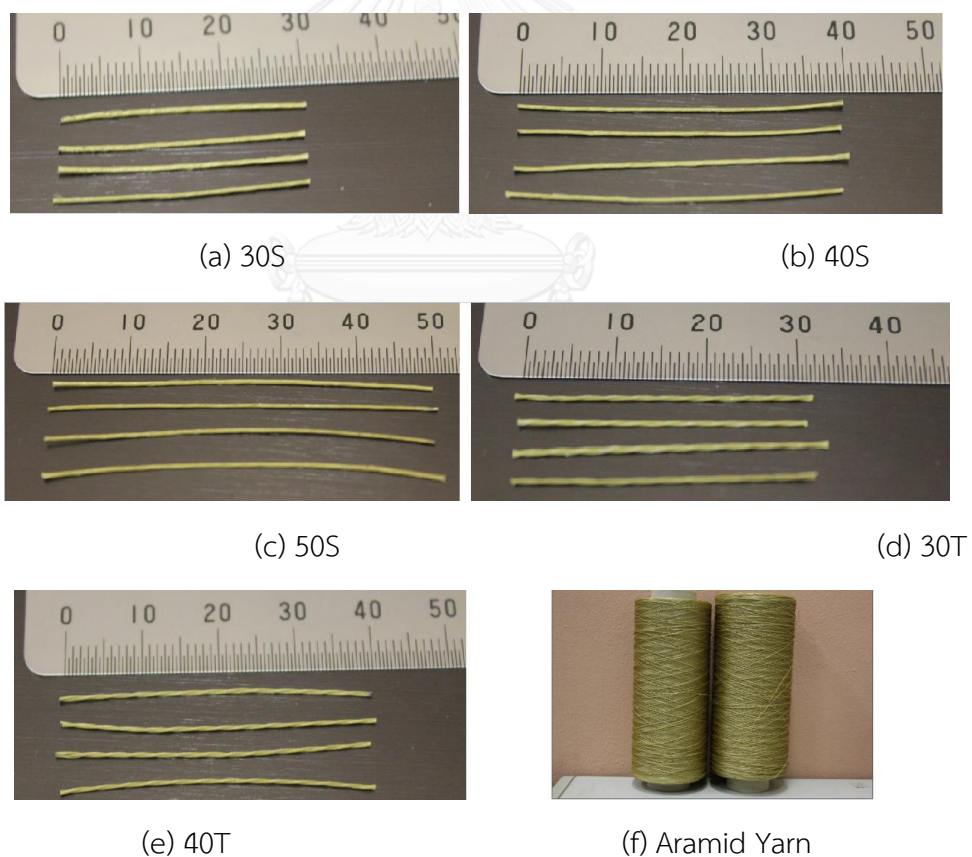


Figure 3.2 Aramid fibers

For AFRC, five different mixtures were prepared varying fiber length (30, 40 and 50 mm) and fiber shape (twist and single). The five types of fibers are presented in **Fig. 3.2**. **Table 3-3** summarizes properties of aramid fibers and the specimen names. The aspect ratio L_f/D_f (ratio between fiber length and diameter) was equal to 60, 80, and 100. All of types of fibers has the same diameter of 0.5 mm. Twist fibers made from two single fibers twisted together, as shown in **Fig. 3.3**. Volume fraction of fibers was 1.0% of concrete volume for all AFRC mixtures.

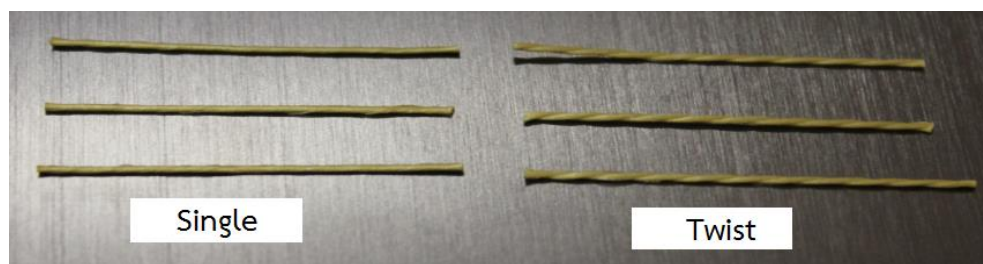


Figure 3.3 Single and twist fibers

Table 3-1 Mix proportion of 1-m³ PC (kg/m³).

w/b ¹⁾	Cement (kg)	Fly ash (kg)	Aggregate (kg)	Sand (kg)	Water (kg)	SP ²⁾ (g)
0.48	324.4	81.1	1016.5	827.7	194.8	1213.3

¹⁾Water/ (cement + fly ash), ²⁾ Super plasticizer

Table 3-2 Mix proportion of 1-m³ AFRC (kg/m³).

w/b ¹⁾	Cement (kg)	Fly ash (kg)	Aggregate (kg)	Sand (kg)	Water (kg)	SP ²⁾ (g)	Aramid fiber
0.48	324.4	81.1	1016.5	827.7	194.8	3447.8	1%

¹⁾Water/ (cement + fly ash), ²⁾ Super plasticizer

3.2.2 Specimens

Specimens were prepared using metallic molds. Eighteen cylinder specimens having dimensions 150x300 mm, three specimens for each mixture, designated for compressive test. Eighteen cylinder specimens having dimensions 150x300 mm, three specimens for each mixture, designated for splitting test. Eighteen dumbbell specimens having dimension as shown in **Fig. 3.4**, three specimens for each mixture, designated for direct tensile test. Twenty-four hours after casting, the specimens were taken out of molds and cured in standard conditions. Specimens were taken out of curing room before 24 hours before tests started.

Table 3-3 Geometry parameters of aramid fibers

Fiber Name	Length, L_f (mm)	Diameter, D_f (mm)	L_f/D_f	Shape
30S	30	0.5	60	Single
40S	40	0.5	80	Single
50S	50	0.5	100	Single
30T	30	0.5	60	Twist
40T	40	0.5	80	Twist

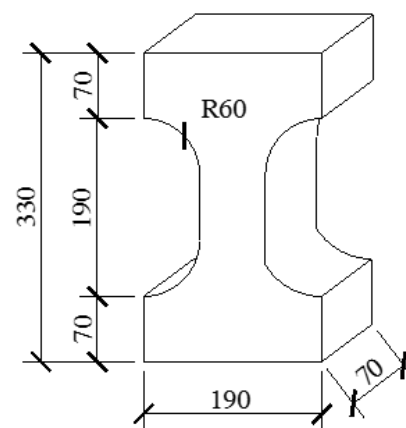


Figure 3.4 Dumbbell specimen [Unit: mm]

3.2.3 Experimental equipment and test procedures

The entire experiment took place at the concrete laboratory of Department of Civil Engineering, Chulalongkorn University. The requirement to mix aramid fiber reinforced concrete is concrete mixer that has high speed to guarantee mixing within three or four minutes. The cause for this problem is that avoiding aramid fiber to produce branching in mixing process.

3.2.3.1 Compressive and splitting test

Compression tests conducted on a Material Testing System (MTS) with a load capacity of 3000 kN. Total of eighteen cylinder specimens were tested in accordance with ASTM C-39 standard [19]. The peak load was recorded during the test.

Split-cylinder tests were carried out in accordance with ASTM C-496 standard [20]. Each cylinder specimen was placed on its side and loaded in compression along a diameter of specimen.

3.2.3.2 Direct tensile test

Direct tensile tests were performed to measure the tensile stress-displacement and ultimate tensile strength according to [21]. Tests were conducted using an Instron 7386C Machine with loading rate of 0.5 mm/min. Two electric displacement transducers were attached to both sides of the center of the tensile specimen in order to monitor the elongation. Equipment setup shows in **Fig. 3.5**.

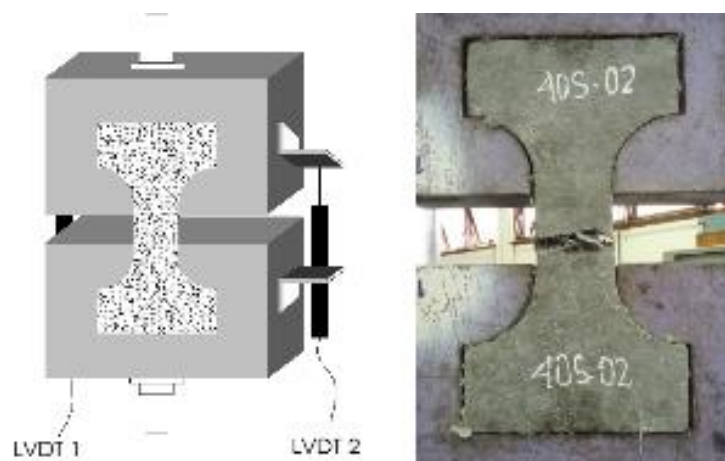


Figure 3.5 Direct tensile test

Testing time of all specimens is around 15 to 16 minutes until each part is completely separated. The first cracks, shape of cracks and cracks position were recorded during the testing.

3.3 Flexural repairing of corroded RC beams by aramid fiber mortar and market product

3.3.1 Material properties

3.3.1.1 Concrete

The targeted compressive strength after 28 days was 30 MPa. The actually concrete compressive and splitting tensile strength were determined based on the average values of three cylinder specimens (150x300 mm) for each tested specimen. The cylinders were cast from the same batch use for casting the specimens. The cylinders and specimens were tested on the same day of testing of specimens. The average concrete compressive, splitting tensile strength of concrete cylinders is 32 MPa and 2.73 MPa respectively.

3.3.1.2 Steel reinforcement

The compressive reinforcement and stirrups were used to be RB6 and RB9, respectively.

Table 3-4 The mechanical properties of the reinforcing bars.

Size	Cross-sectional area (mm ²)	Grade	Modulus of Elasticity (MPa)	Yield strength (MPa)	Ultimate strength (MPa)	Mass per m (kg/m)
DB16	201.06	SD40	200,000	537.2	673.9	1.578
RB9	63.60	SR24	200,000	235	385	0.499
RB6	28.30	SR24	200,000	235	385	0.222

The steel reinforcing bars conformed to the requirement of the TIS (Thailand Institute Steel) standard for deformed bars were tested to obtain their mechanical properties. The yield stress and the ultimate strength of the longitudinal reinforcing DB16 (SD40) were found to be 537.15 MPa and 673.93 MPa, respectively. The steel reinforcement was used in specimens as shown in Table 3-4.

3.3.1.3 Aramid fibers reinforced mortar

Aramid fibers reinforced mortar was used as a material to strengthen RC beam. The mix-design for aramid fibers reinforced mortar shown in **Table 3-5**. Water to cement ratio has been set to 0.40. Sand, ordinary Portland cement (OPC) and super plasticizer (Type: Master Glenium ACE 8320) has been used. Aramid fibers type forty millimeters long with twist shape were used in this proportion. The volume fraction of fibers was 1.0%.

Table 3-5 Mix proportion of 1-m³ AFRM (kg/m³).

w/c	Cement (kg)	Sand (kg)	Water (kg)	Super-plasticizer (g.)	Aramid fiber V _f (%)
0.4	628.74	1414.67	251.49	6287.43	1.0

The mortar compressive strength was determined based on the average values of six cubes specimens (50x50x50 mm). The average mortar compressive strength is 56.53 MPa after 14 days.

Another means of concrete tensile strength determination is the briquette tensile test. This test method involves two types of shapes. The small dumbbell briquette is 76 mm long, 25 mm thick, 625 mm² cross section at the mid-length and other dumbbell briquette is 330 mm long, 70 mm thick, and 490 mm² cross section at the mid-length as shown in **Fig 3.6**.

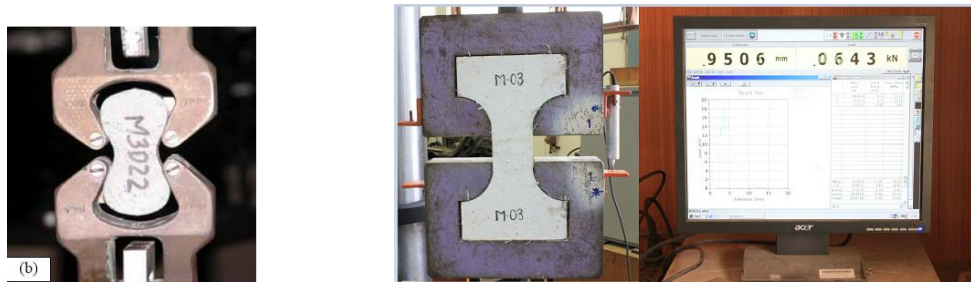


Figure 3.6 Dumbbell briquette

The average tensile strength of five small dumbbell briquette is 7.73 MPa after 14 days. For larger dumbbell briquette, the results were recorded by computer. The results indicate the relationship of stress and strain of aramid reinforced mortar as shown in **Fig. 3.7**. The behaviour of specimens were determined based on the average values of three dumbbell specimens. The ultimate tensile strength of aramid fibers reinforced mortar is 2.82 MPa. The maximum post-cracking tensile strength is 2.70 MPa.

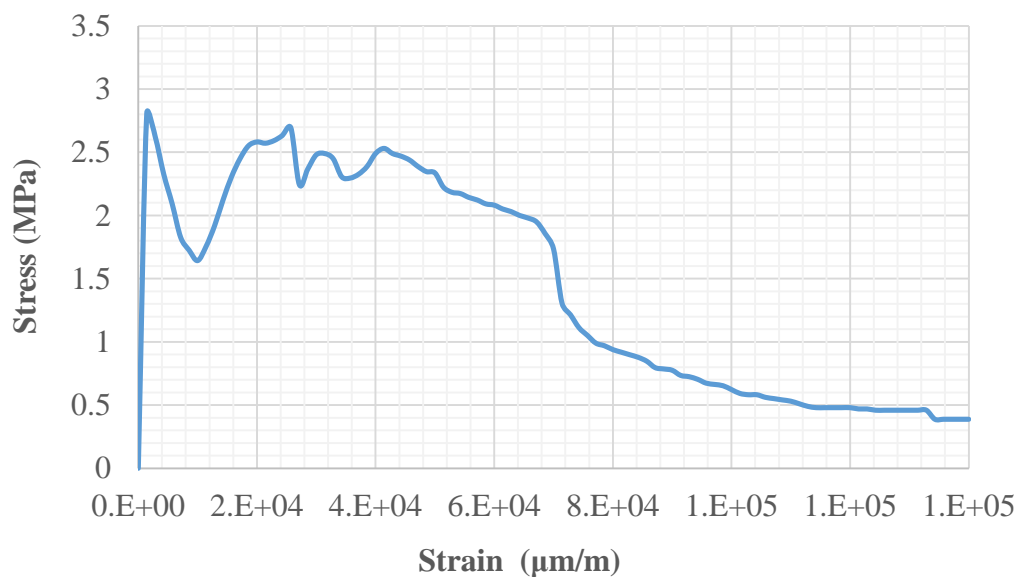


Figure 3.7 Stress-strain relationship of AFRM

3.3.1.4 Market product

Other material was used to strengthen RC beam what it was a product available in market. The mortar compressive strength was determined based on the average values of six cubes specimens (50x50x50 mm). The average mortar compressive

strength is 32.71 MPa after 14 days. The tensile strength determination is small dumbbell briquette. The average tensile strength based on five specimens is 3.76 MPa after 14 days.

3.3.2 Specimen layout and detail

Four beams were carried out having dimension as 150x200x1400 mm. The detail of the beam shown in **Fig. 3.8**. The cover concrete equal 20 mm for all sides. Two longitudinal reinforce DB16 were arranged at the tension section and two longitudinal reinforce RB6 were arranged at compression section for each beam. The stirrups were used be RB9 with spacing of 60 mm. Stirrups were covered by plastic tape at the contact point with longitudinal reinforcing bar to avoid corrosion of stirrups.

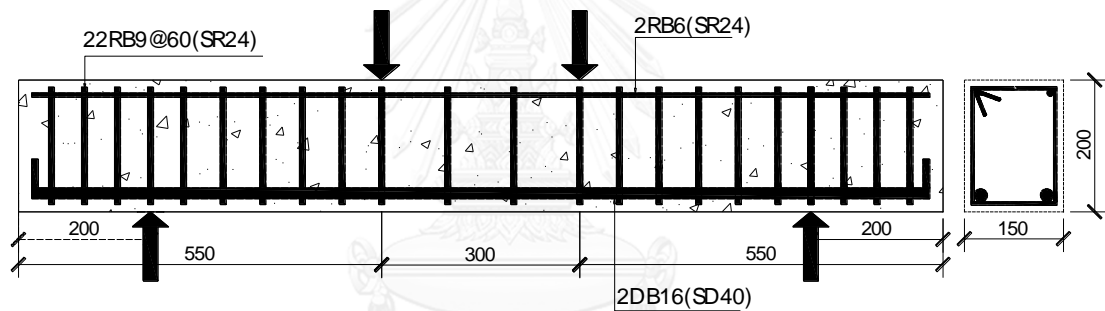


Figure 3.8 Dimensions and reinforcement details of the beam test specimen

Table 3-6 Details of beam specimens

No.	Beam ID	Corroded expectation	Strengthening
1	BC	-	-
2	NRB	10%	-
3	SB-AFM	10%	By aramid fibers reinforced mortar
4	SB-MP	10%	By product available in market

All of the sections considered here were under-reinforced to obtain the preferred type of flexural behaviour. Each beam investigated different parameters as shown in

Table 3-6. Beam named BC as a control beam. Three beams were corroded expectation 10% mass losses. While NRB beam were unstrengthen. Beam SB-AFM was strengthened by aramid fibers reinforced mortar and beam SB-MP was strengthened by product available in market.

3.3.3 Accelerated corrosion test

The watertight tanks of 2000x1000x400 mm, was built as a part of the facility required for the process of accelerated corrosion. **Figure 3.9** illustrates schematic diagram of the corrosion test set up. The external cathode constructed from 6-mm diameter steel. The main reinforcement connected to the power supplies by a lead wires. To assure the similarity of two main reinforcements, they were connected by a welded-wire.

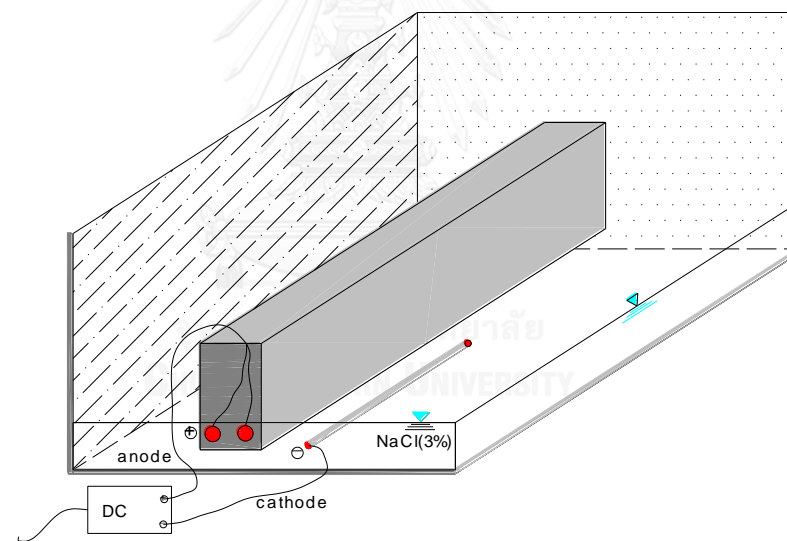


Figure 3.9 Corrosion test set up

Specimens were submerged to their one-third depths into 3% NaCl. The evaporation will occur. Therefore, water was refilled to assure that NaCl aqua reaches one-third depth of beams in corrosion process. The electric current was impressed for three beams as well as recorded after one hour. **Table 3-7** summarizes the total time and electric current for each beam.

Table 3-7 The total time and electric current for corrosion test

No.	Beam ID	Initial current (A)	Average current (A)	Total time (h)	Hour x Ampere (H.A)
1	NRB	5.95	6.98	84.83	592
2	SB-AFM	5.73	7.25	82.75	600
3	SB-MP	5.71	7.22	83.38	602

3.3.4 Repairing procedures

3.3.4.1 Breaking damaged concrete

Two beams broke damaged concrete. The distance for breaking is 70 mm from extremely tension fiber. Breaking procedure illustrated in **Fig. 3.10**.



Figure 3.10 Breaking tension zone

3.3.4.2 Soaking corroded reinforcement

Two beams which were damaged concrete were cured at 60° in 10% diammonium hydrogen citrate for 2 days to clean the rust around reinforced bars. Curing procedure illustrated in **Fig. 3.11**.



Figure 3.11 Soaking broken-beam

3.3.4.3 Repairing beams by AFRM and product available in market

Two beams were set-up and casted as show in **Fig. 3.12**. Steel strain gauges were attached at the same position with other beams. The repairing part were rotated as show in **Fig. 3.12** to make sure the height 200 mm for each beam.

Lanko 751 was used as the bonding between old concrete and fresh mortar. After curing 14 days, four beams were conducted four-point flexural beam test.



(a) Repairing set-up

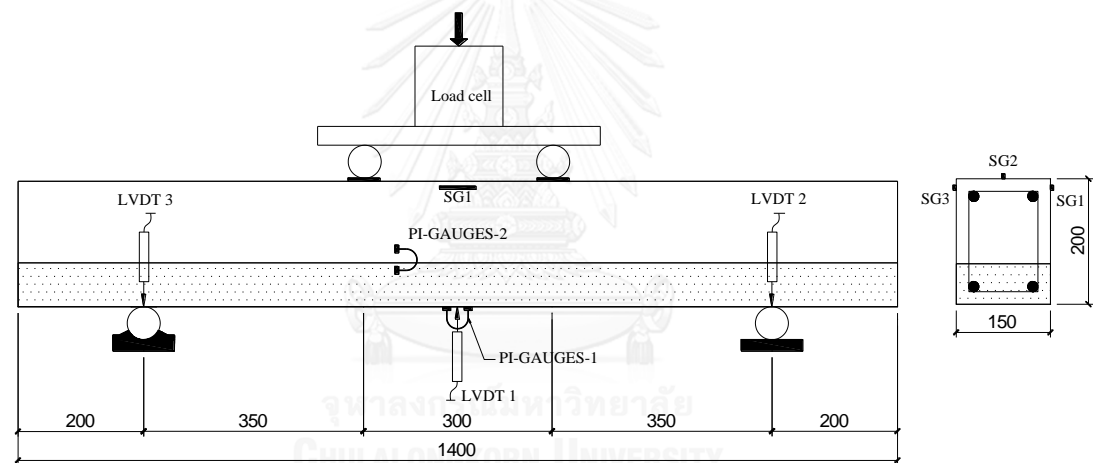


(b) Casting

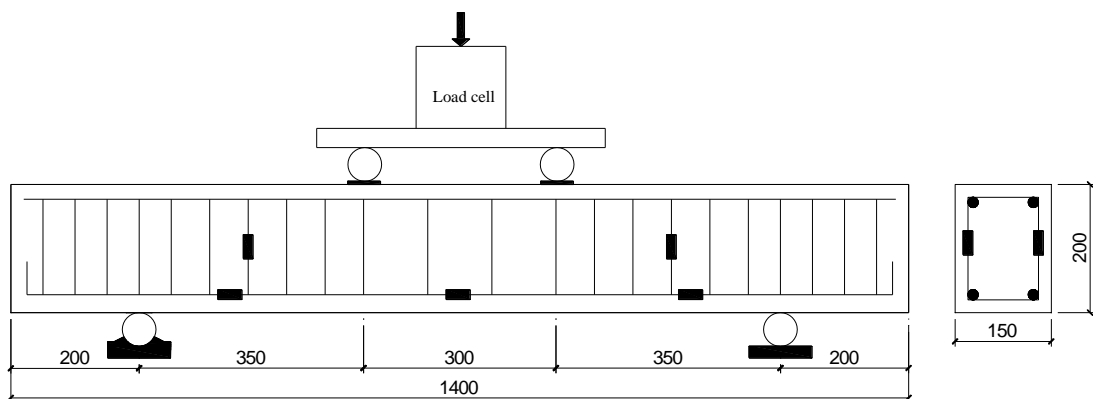
Figure 3.12 Repairing beam by AFRM and mortar product in the market

3.3.5 Test set up

Four specimens will be carried out load test. The linear variable differential transducers (LVDTs) were set at the midspan and supports to measure the vertical displacements. On the top of beams, at the loading points, gypsum was pasted to make the balance level of two loading points. Pi-gauges I attached at the middle bottom of each beams. However, for two repairing beams, there attached other Pi-gauges to dedicate the width of bonding. Concrete strain gauges were attached at the compressive zone to measure compressive strain at the middle of the beam. Moreover, steel strain gauges were attached the steel cages as show in **Fig. 3.13 (b)**. All of measurement were connected with data logger to record the results of entire test.



(a) Set-up LVDTs, PI Gauges, and concrete strain gauges



(b) Location of steel strain gauges



(c) Four point flexural beam test

Figure 3.13 Experimental setup

Chapter 4

EXPERIMENTAL RESULTS AND DISCUSSION

4.1 General

This chapter presents the experimental results for two stages:

Stage 1: The mechanical properties of aramid fiber reinforcement concrete (AFRC).

Stage 2: The flexural behaviour of RC beams strengthened by aramid fiber reinforced mortar and product available in the market.

Plain concrete (PC) and five types AFRC with the different of shapes, lengths were studied. Compressive, splitting test and direct tensile test were conducted. The mechanical properties of AFRC will be discussed through compressive, splitting strength, ultimate tensile strength and post-cracking characteristics of PC and AFRC type. Thereby, the satisfied parameter aramid fiber was selected as a material to strengthen corroded beams in stage 2.

Four beams with dimension 1400x200x150 mm were carried out. Three beams were expected approximately 10% of accelerated corrosion to longitudinal reinforcement. One corroded beam was strengthened by aramid fibers reinforced mortar and other corroded beam by product available in market. In each beam, the flexural behaviour of RC beam will be discussed though cracking load, yielding load, ultimate load and displacement respectively, flexural stiffness, strain in concrete, reinforcement as well as displacement of layer between old concrete and new mortar. In addition, the crack width, number of cracks and failure modes will be discussed in this chapter.

4.2 Mechanical properties of aramid fibers reinforced concrete

4.2.1 Compression and splitting strength

Compressive strength is summarized in **Table 4-1** and showed in **Fig. 4.1**. The 30-mm fiber with single shape (30S) gave the highest compressive strength ($f_c' = 41.2$ MPa). Compressive strength of fibers having the same length is nearly the same.

Table 4-1 Compressive strength and splitting strength results

No.	Name	Compressive Strength, f_c' , (MPa)	Splitting Strength, f_{ct} (MPa)
1	PC	39.50	2.40
2	30S	41.20	3.78
3	40S	34.03	3.83
4	50S	32.41	4.23
5	30T	35.86	4.07
6	40T	35.35	3.74

However, failure mode considerably changed from fragile to ductile because of the bridging effect of the fibers when compared with plain concrete. Multiple fine cracks were visually observed after the compressive test. The results of compressive test showed that compressive strength is less different of between five types of aramid fibers and plain concrete.

The splitting tensile strength, f_{ct} , from a split-cylinder test presents the variations on the effect of fiber length. It is observed from the test results given in **Table 4-1** that there is modest improvement in the splitting tensile strength due to increase in fiber length from 30 mm to 50 mm. The highest splitting tensile stress is 4.23 MPa belonging to 50-mm fibers. For the plain concrete, the tensile strength of concrete falls 6 percent of the compressive strength. However, the tensile strength of AFRC is approximately 9 to 14 percent of its compressive strength. Therefore, splitting

tensile testing clearly indicates that having significant improvement splitting tensile strength with the presence of aramid fiber in concrete.

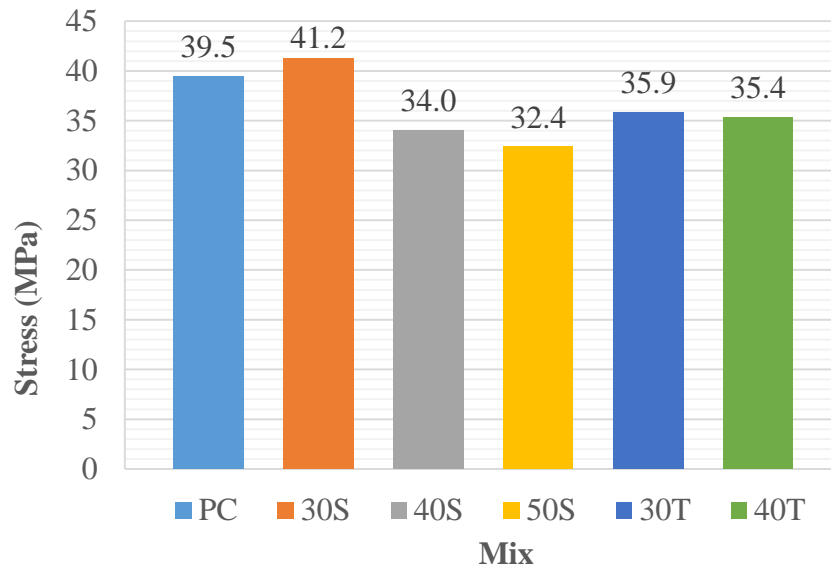


Figure 4.1 Compressive strength

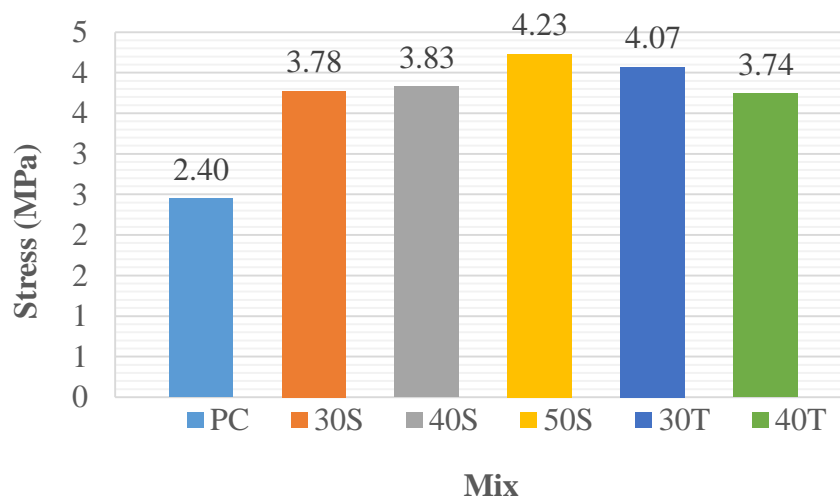


Figure 4.2 Splitting tensile strength

4.2.2 Direct tensile strength

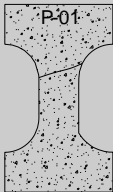
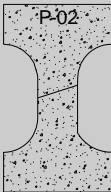
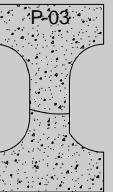
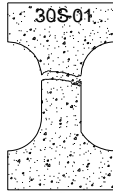
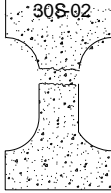


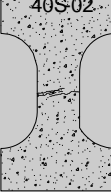
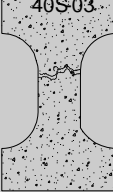

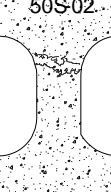
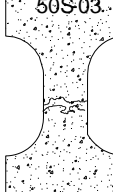
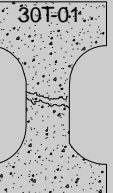
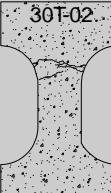
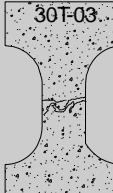
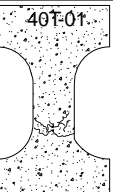
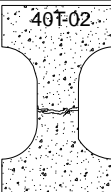
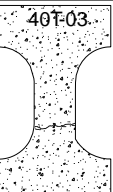
Direct tensile tests were dedicated ultimate tensile strength of concrete. **Table 4-2** show the peak load of five types of AFRC and plain concrete. Plain concrete is brittleness, it easily separated to two parts after the peak load. For AFRC, even though the cracks occurred in the specimens but it still resisted the loads. The results indicated that with the presence of fibers, the tensile failure of AFRC turned from brittleness to toughness.

As show in **Table 4-2** and **Fig. 4.4**, the results indicated a modest increase in first cracks and maximum strength of plain concrete and AFRC while the ability to absorb energy in the post-crack region improved significantly with the addition aramid fibers in concrete.

The mode failure includes two types: rupture and pull out. **Figure 4.3** show the section of dumbbell specimens after failure. **Figure 4.3 (a)** with circle marks shows the rupture failure. **Figure 4.3 (b)** with rectangular marks shows the pull-out failure. Rupture failure was displayed by branching fiber (with many filaments fiber) and pull-out failure was displayed the original shape of fiber. Although aramid fiber itself had high tensile strength, aramid fibers was broken in concrete while tensile stress was around 1.5 to 2.95 MPa. It may cause by the difference of the resistance load which each filaments resists (one fiber consists of many filaments). Each filament ruptured first and leded to totally fiber ruptured.

Aramid fiber has perfectly bonding with concrete. Therefore, when long fibers are able to provide the sufficient embedded length, layers of concrete pulled contemporaneously with fibers. Meanwhile, specimens occur many cracks especially in specimens have twist fibers.

Table 4-2 Direct tensile results

Name	Peak Load (kN)	Specimens after failure
PC-01	7.70	
PC-02	10.03	
PC-03	Error ³⁾	
30S-01	11.87	
30S-02	7.09	
30S-03	12.09	
40S-01	15.39	
40S-02	8.78	
40S-03	14.03	
50S-01	8.09	
50S-02	10.11	
50S-03	15.2	
30T-01	6.75	
30T-02	9.34	
30T-03	5.75	
40T-01	9.03	
40T-02	11.3	
40T-03	12.59	

³⁾ Broken during installation

Stress and displacement relationships are shown in **Fig. 4.4**. It can be seen that after occurring cracks, all AFRC specimens still resist the load (50 to 66 percent comparing with peak load). This has significant implications at the composite level

where cracks can be constrained by the fibers up to very large crack widths [22]. Maximum loads occur at deflection = 0.1 to 0.3 mm. Fibers with 40 mm long and single shape (40S) provided the highest tensile strength. The tensile strength was 2.95 MPa when the deflection was 0.1 mm.



(a) Rupture failure of 40S specimen



(b) Pull-out failure of 40S specimen

Figure 4.3 Mode failure of AFRC

Figure 4.5 presents the effect of fiber length on the stress – displacement curves. The results of single-shape AFRC with different fiber length ($L_f = 30, 40$ and 50 mm) are plotted together. It can be seen that all specimens are elastic at first stage (displacement = 0 to 0.1 mm).

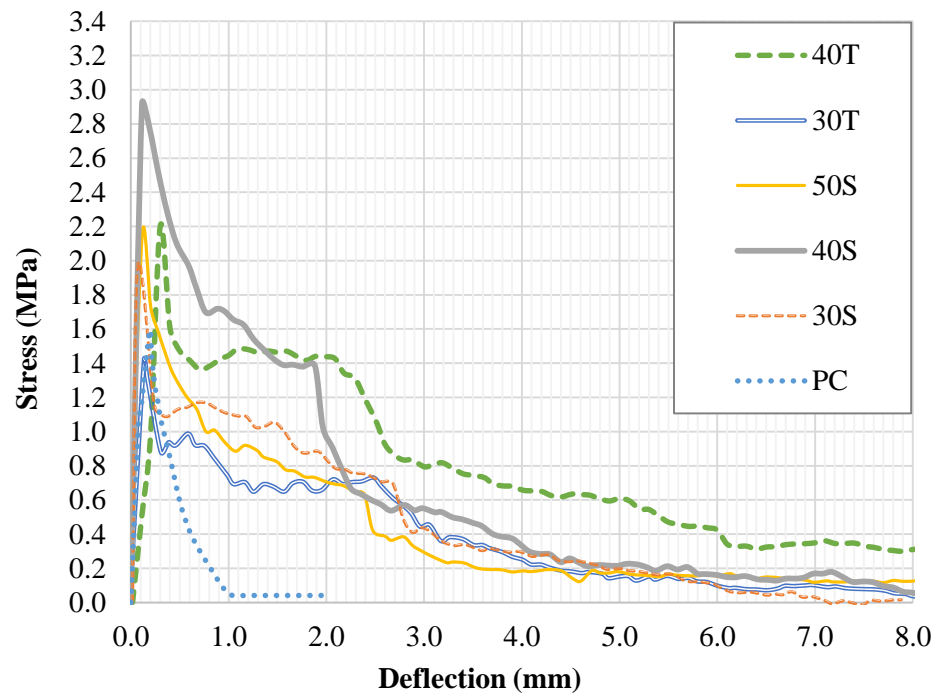


Figure 4.4 Stress – displacement relationship

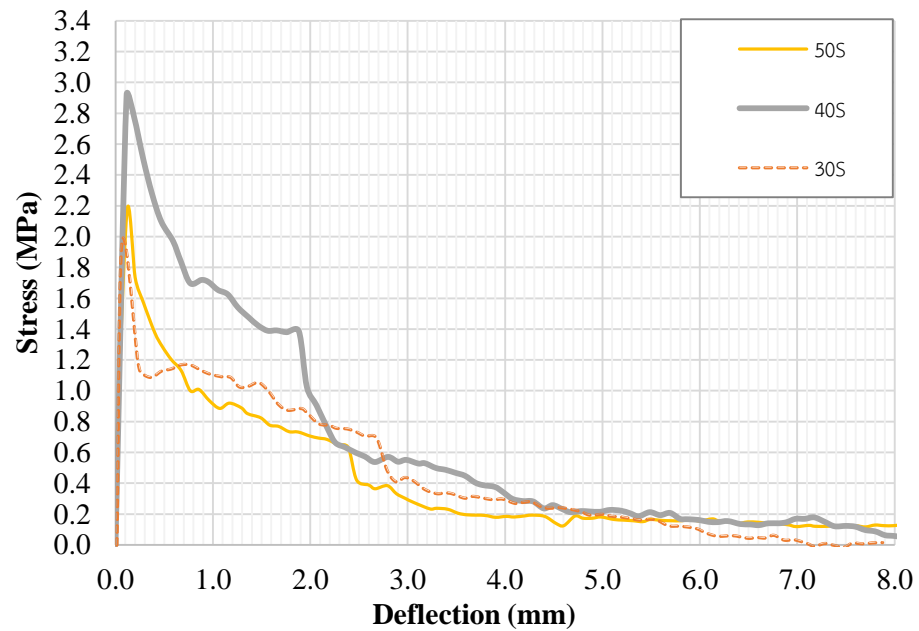


Figure 4.5 Stress – displacement curves of ARFC with different fiber length

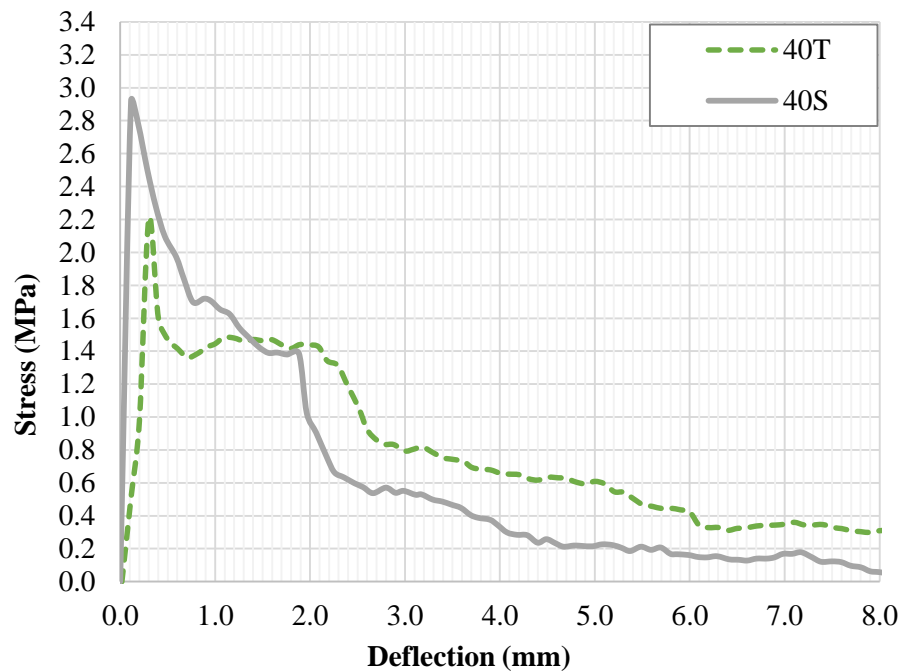


Figure 4.6 Stress – displacement curves of ARFC with different fiber shape

By observing the failure section of all 30-mm fibers experiments, most of fibers was pulled-out. It indicates that fibers with 30 mm long are not be able to provide the sufficient embedded length in the concrete.

The results of fiber with 50 mm shown in **Fig. 4.5**. Maximum tensile stress is 2.1 MPa. It is quite low value when comparing with another kind of fiber. In addition, in post-peak region, the descending branch of 50S showed downward trend until failure. On the other hand, fibers with 30 mm and 40 mm long are able to resist higher stress in post peak region. Balling may become a problem as fiber length is increased. Balling is very difficult to separate. Therefore, mixing time increase when balling occurring. Fibers split to filaments and led to decrease tensile strength of fibers [23].

According to the experimental results, fibers with 40 mm long provided the highest tensile stress. The maximum tensile stress was 2.2 and 2.9 MPa for the twist and single fibers, respectively. By observing the failure section, the fiber failure was both rupture and pull-out. Therefore, fibers with 40 mm long has sufficient embedded length in concrete and still avoid branching fiber in casting processing concrete.

Figure 4.6 presents the comparison between single and twist fibers. Single fibers have higher tensile stress than twist fibers. However, descending branch of twist fibers are more stable than those of single fibers. As presented in **Fig. 4.6**, after load reached to the peak, a slight drop was found in case of 40T while 40S shown shape drop. Twist fibers resisted load approximately 70 percent of maximum load from 0.8 to 2.2 mm in deflection. There is a beneficial mechanism of twist fibers. Twist shape provides a larger surface area for adhesion and frictional bond than single shape. However, fibers with 30 mm long did not clearly show this beneficial mechanism of twist fibers because of insufficient length of fiber.

Although single and twist fibers have the same diameter, behaviour of each aramid fiber reinforced concrete are different. It is because twisted fibers are not perfectly straight, therefore, when stress occurred in concrete, twist fibers pulled to straight itself and it was not along with concrete to resist the micro cracks, while single fibers can resist the propagation of crack immediately. The second reason is that twist fibers are easier segregation than single fibers. As previous assumption, the rupture was occurred at each filament fiber. It leads to the rupture of total fibers. This is the reason why specimens with twisted fibers cracked before single ones.

4.3 Test results and discussion of RC Beams

4.3.1 Accelerated corrosion result

4.3.1.1 Concrete damage condition

During the corrosion process, the test specimens in the watertight tank were inspected approximately at 84 hours. **Figures 4.7 - 4.9** show the crack patterns and crack width of four specimens.

Two cracking patterns were observed: In the first pattern, longitudinal cracks appeared at the bottom soffit parallel to the main reinforcement bars and a second longitudinal crack appeared on one side fascia as shown in **Fig. 4.7**. In the second pattern, longitudinal cracks appeared at the bottom soffit parallel to the main reinforcement bars, but no crack was observed on the side fascia as shown in **Fig. 4.8** and **Fig. 4.9**.

For beam repairing by aramid fibers reinforced mortar, SB-AFM, there has two longitudinal cracks which occur at two sides (bottom soffit and side fascia). At the bottom soffit, there is one longitudinal crack and the maximum crack width 1.40 mm was observed. At the side fascia, there is one longitudinal crack and the maximum crack width 0.80 mm was observed.

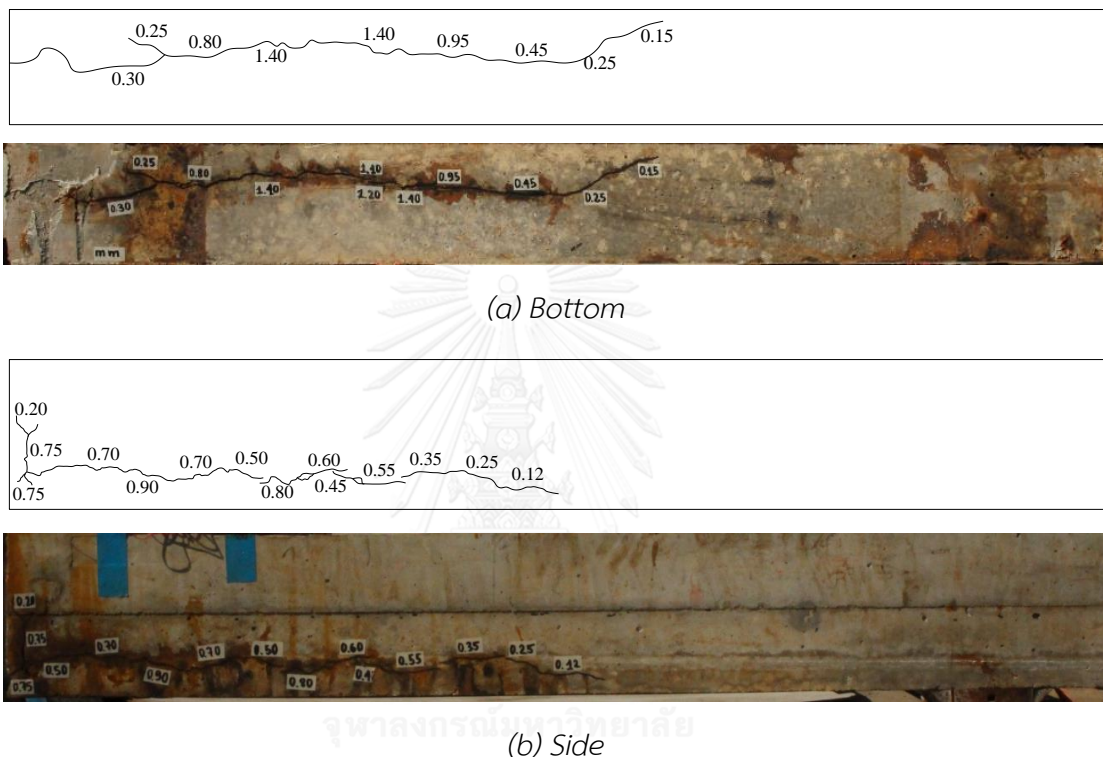


Figure 4.7 Crack pattern and crack width of SB-AFM beam (unit: mm)

For corroded beam without repairing, NRB, there has two parallel longitudinal cracks at the bottom soffit. The cracks occurred at the entire bottom side. The maximum crack width 0.95 was observed.

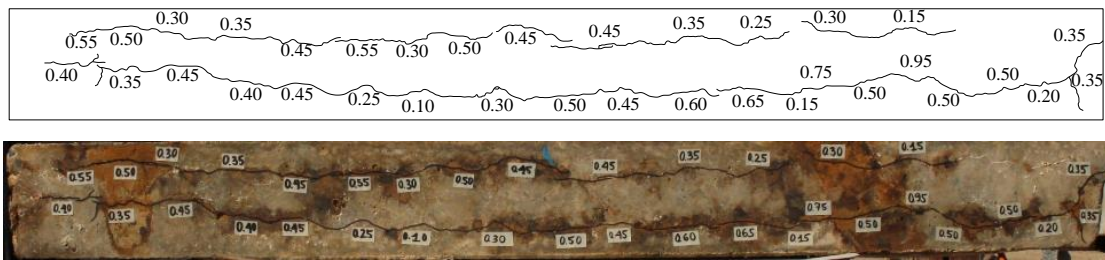


Figure 4.8 Crack pattern and crack width of NRB beam at the bottom (unit: mm)

For beam repairing by mortar product available in the market, SB-MP, there has one longitudinal crack at the bottom soffit. The maximum crack width 0.45 mm was observed. Moreover, there hole with 2.0 mm diameter was observed in this beam.

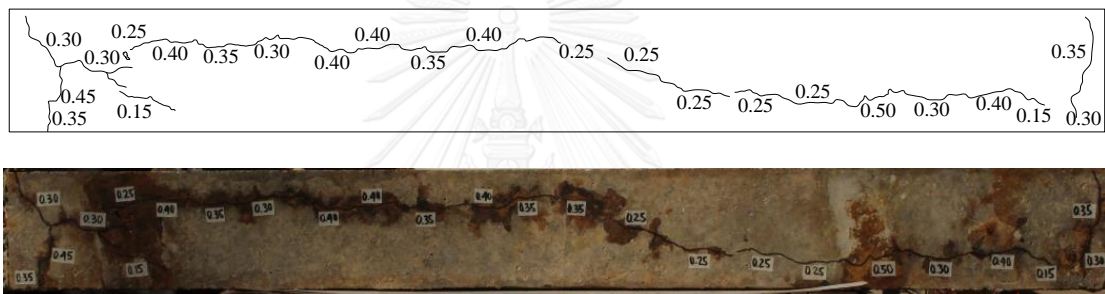


Figure 4.9 Crack pattern and crack width of SB-MP beam at the bottom (unit: mm)

4.3.1.2 Steel damage condition

The corrosion mostly attacked transverse and longitudinal ribs of longitudinal bars as shows in **Fig. 4.10 (a)**. However, corrosion occurred non-uniformly over a particular area of longitudinal bars as shown in **Fig. 4.10 (b)**.

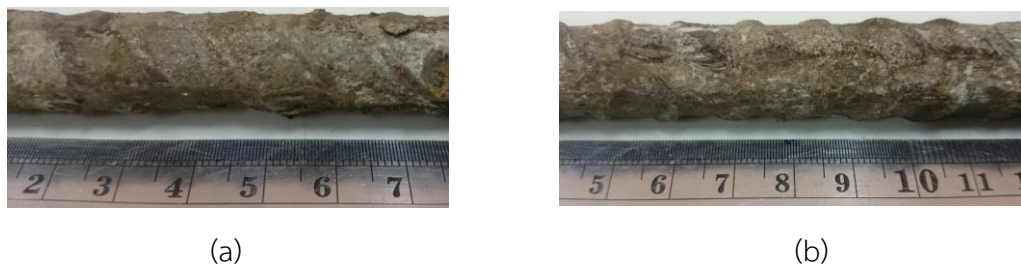


Figure 4.10 Surface of corroded reinforced bars

The mass of corroded longitudinal bars is compared with un-corroded longitudinal bars to estimate the amount of mass lost because of corrosion. The maximum mass loss measured was 10.63%, the minimum was 9.18% and the average mass loss was 9.95%. **Table 4-3** shows the mass loss of corroded beams.

Table 4-3 Mass loss

Beam ID	Mass Loss (%)
BC	-
NRB	10.05
SB-AFM	9.18
SB-MP	10.63

4.3.2 Flexural repairing RC beams

4.3.2.1 Load- deflection behaviour and failure mode

During bending process, the load deflection behaviour of a reinforced concrete beam consist of three stages: pre-cracking stage, pre-yielding and post-yielding until failure. These stages are identified by the cracking and yielding load. **Figure 4.11** shows the load-deflection behaviour of reinforced concrete beams at different stages of loading.

The cracking load, P_c , is defined as a load at which the tensile stress at the bottom of the beam is greater than the concrete tensile strength. The cracking load was obtained from observing in test process of each beam. The yield load, P_y , is defined as the load at which the tensile steel yields. The yield load was obtained from the load- deflection curves relationship of each beam. This lead to the formation of the flexural cracks and reduction in the beam flexural stiffness. The ultimate load, P_u , is defined as the load at which the load drops due to beams failure and it is concrete crushing for all beams as shown in **Fig. 4.12**.

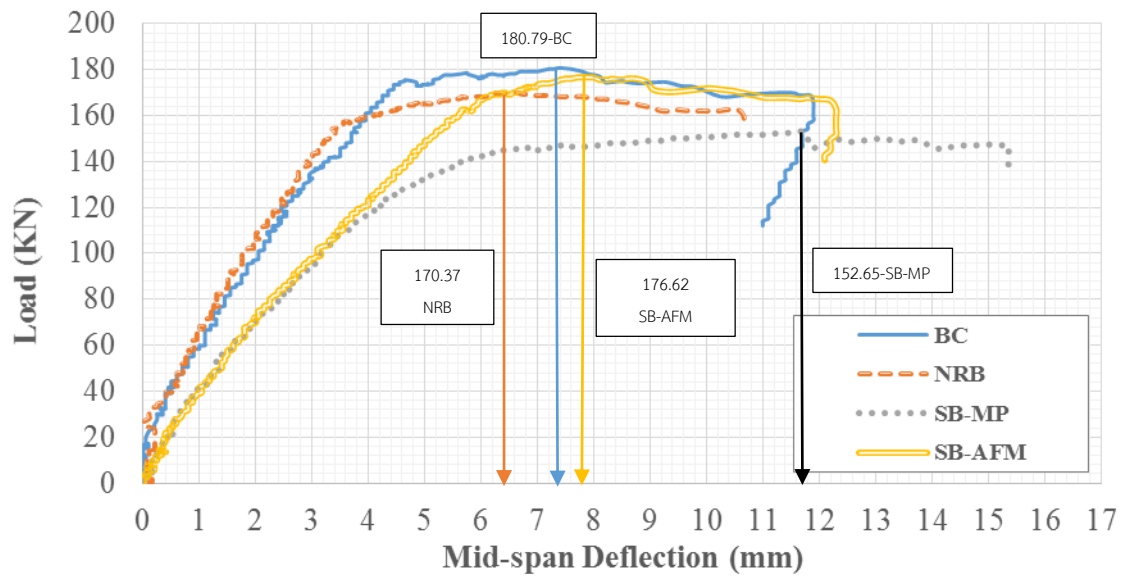


Figure 4.11 Load-midspan deflection behaviour



Figure 4.12 Concrete crushing failure

Table 4-3 presents material properties of the RC beams. The load and deflection detail for four beams are summarized in Table 4-4.

At the pre-cracking state, beam control (BC) was working the same behaviour with non-repairing beam, NRB and two repairing beams have the same behaviour. Although cracking load of BC and NRB beam has slightly higher than SB-AFM and SB-MP, the deflection at cracking point (Δ) of SB-AFM and SB-MP has significant increasing as show in Table 4-4 and Table 4-5.

Table 4-3 Material properties of all the beams

Beam ID	Material repairing					
	Concrete		Aramid fiber reinforced mortar		Mortar product in the market	
	f_c' (MPa)	f_{ct} (MPa)	f_c (MPa)	f_t (MPa)	f_c (MPa)	f_t (MPa)
BC	32	2.73	-	-	-	-
NRB	32	2.73	-	-	-	-
SB-AFM	32	2.73	56.53	7.73	-	-
SB-MP	32	2.73	-	-	32.71	3.76
Dimension specimen	Cylinder 150x300		Cube 50x50x50	Small dumbbell briquette	Cube 50x50x50	Small dumbbell briquette

Table 4-4 The test results of all the beams

Beam ID	Crack state		Yielding state		Ultimate state		Failure Mode
	Load (kN)	Δ (mm)	Load (kN)	Δ (mm)	Load (kN)	Δ (mm)	
BC	35	0.4	172	4.45	180.79	7.40	Concrete crushing
NRB	40	0.5	157.34	3.55	170.37	6.55	Concrete crushing
SB-AFM	40	1.05	161.51	5.65	176.62	7.80	Concrete crushing
SB-MP	20	0.45	133.9	5.10	152.65	11.75	Concrete crushing

Table 4-5 Comparison of load

Beam ID	Cracking load			Yield load			Ultimate load		
	P_c (kN)	$P_c/P_c(BC)$	$P_c/P_c(NRB)$	P_y (kN)	$P_y/P_y(BC)$	$P_y/P_y(NRB)$	P_u (kN)	$P_u/P_u(BC)$	$P_u/P_u(NRB)$
BC	35	1.00	-	172.00	1.00	-	180.79	1.00	-
NRB	40	1.14	1.00	157.34	0.91	1.00	170.37	0.94	1.00
SB-AFM	40	1.14	1.00	161.51	0.94	1.03	176.62	0.98	1.03
SB-MP	20	0.57	0.50	133.90	0.78	0.85	152.65	0.84	0.89

Table 4-6 Comparison of deflection

Beam ID	Deflection at cracking point			Deflection at yielding point			Deflection at ultimate load point		
	Δ_c	$\Delta_c/$	$\Delta_c/$	Δ_y	$\Delta_y/$	$\Delta_y/$	Δ_u	$\Delta_u/$	Δ_u/Δ_u
	<i>mm</i>	$\Delta_{c(BC)}$	$\Delta_{c(NRB)}$	<i>mm</i>	$\Delta_{y(BC)}$	$\Delta_{y(NRB)}$	<i>mm</i>	$\Delta_{u(BC)}$	$\Delta_{u(NRB)}$
BC	0.40	1.00	-	4.45	1.00	-	7.40	1.00	-
NRB	0.50	1.25	1.00	3.55	0.79	1.00	6.55	0.88	1.00
SB-AFM	1.05	2.62	2.10	5.65	1.27	1.59	7.80	1.05	1.19
SB-MP	0.45	1.12	0.90	5.11	1.15	1.44	11.75	1.59	1.79

At yield load, BC beam has the highest yield load, 172 kN. The corroded beam has 10% mass loss, the yield load was decreased 9%, 6%, and 22% for NRB, SB-AFM, and SB-MP, respectively. Moreover, yield load of the beam which was repaired by aramid fibers reinforced mortar (SB-AFM) increase 3% comparing with the beam without repairing. However, the yield load of the beam which was repaired by mortar in the market (SB-MP) decrease 15% comparing with the beam without repairing.

At ultimate load, BC beam has the highest yield load, 180.79 kN. The corroded beam has 10% mass loss, the ultimate load was decreased 6%, 2%, and 16% for NRB, SB-AFM, and SB-MP, respectively. Moreover, ultimate load of the beam which was repaired by aramid fibers reinforced mortar (SB-AFM) increase 3% comparing with the beam without repairing. However, the ultimate load of the beam which was repaired by mortar in the market (SB-MP) decrease 11% comparing with the beam without repairing.

Deflection of BC beam is higher than NRB beam 21% at the yield point, and 12% at ultimate point. Deflection of SB-AFM beam is higher than BC beam 27% at the yield point, and 5% at ultimate point and is higher than NRB beam 59% at the yield point, and 19% at ultimate point. Deflection of SB-MP beam is higher than BC beam 15% at the yield point, and 59% at ultimate point and is higher than NRB beam 44% at the yield point, and 79% at ultimate point. For control beam, BC, the load deflection relationship is shown in **Fig. 4.13**. Beam BC cracked at a load of 35 kN, yielded at a

load of 172 kN, and failed at ultimate load of 180.79 kN with mid-span deflection of 0.40 mm, 4.45 mm, and 7.4 mm, respectively. There is increasing 5.11% from yielding to ultimate load.

For corroded beam and repairing by aramid fibers reinforced mortar, SB-AFM, the load deflection relationship is shown in **Fig. 4.15**. Beam SB-AFM cracked at a load of 40 kN, yielded at a load of 161.51 kN, and failed at ultimate load of 176.62 kN with mid-span deflection of 1.05 mm, 5.65 mm, and 7.8 mm, respectively. There is increasing 9.35% from yielding to ultimate load.

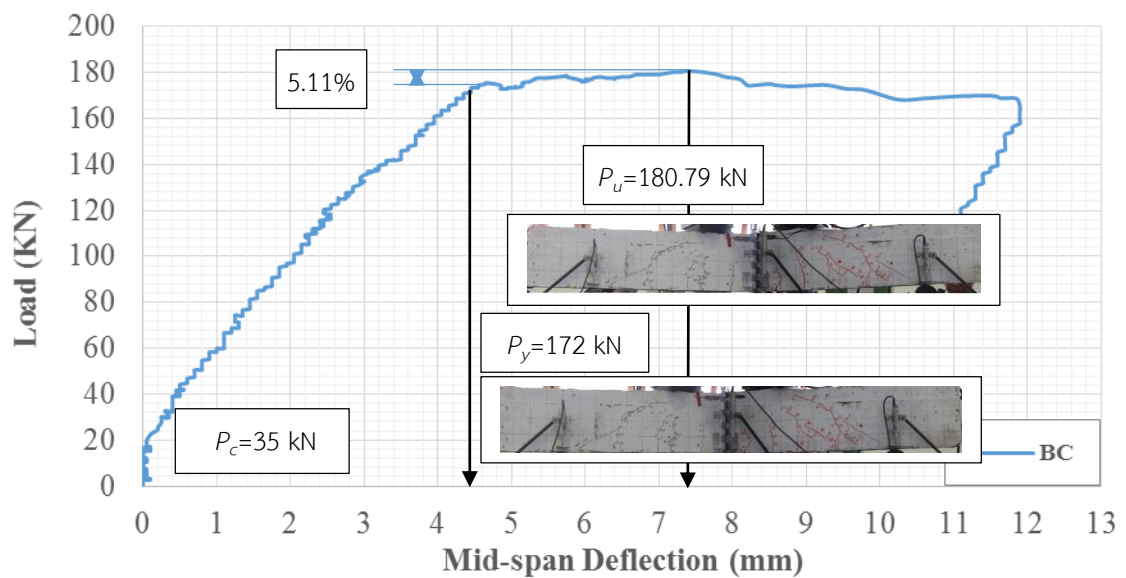


Figure 4.13 Load-midspan deflection behaviour of BC beam

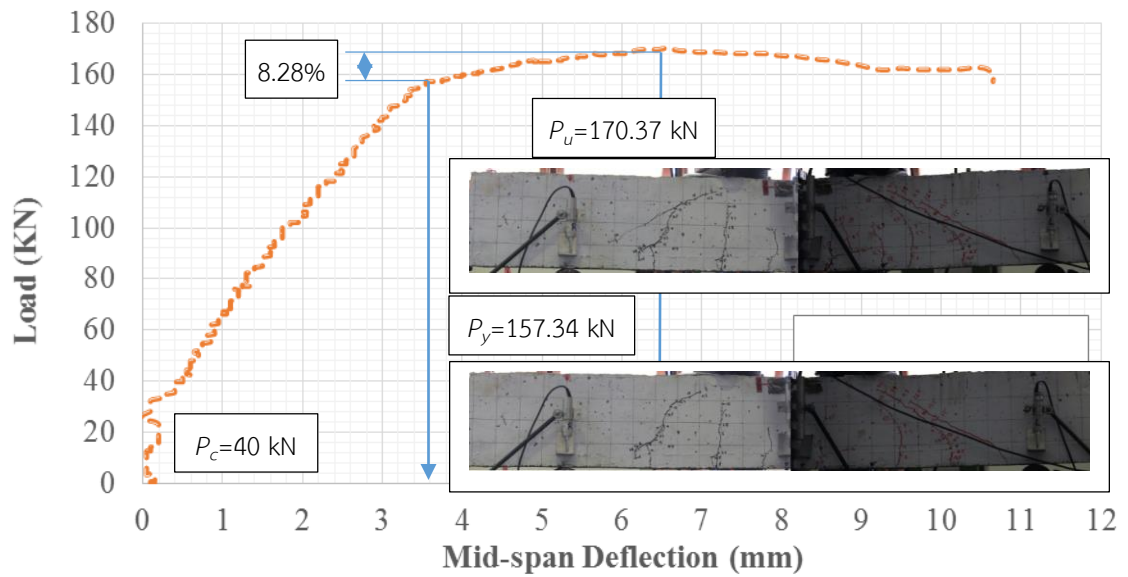


Figure 4.14 Load-midspan deflection behaviour of NRB beam

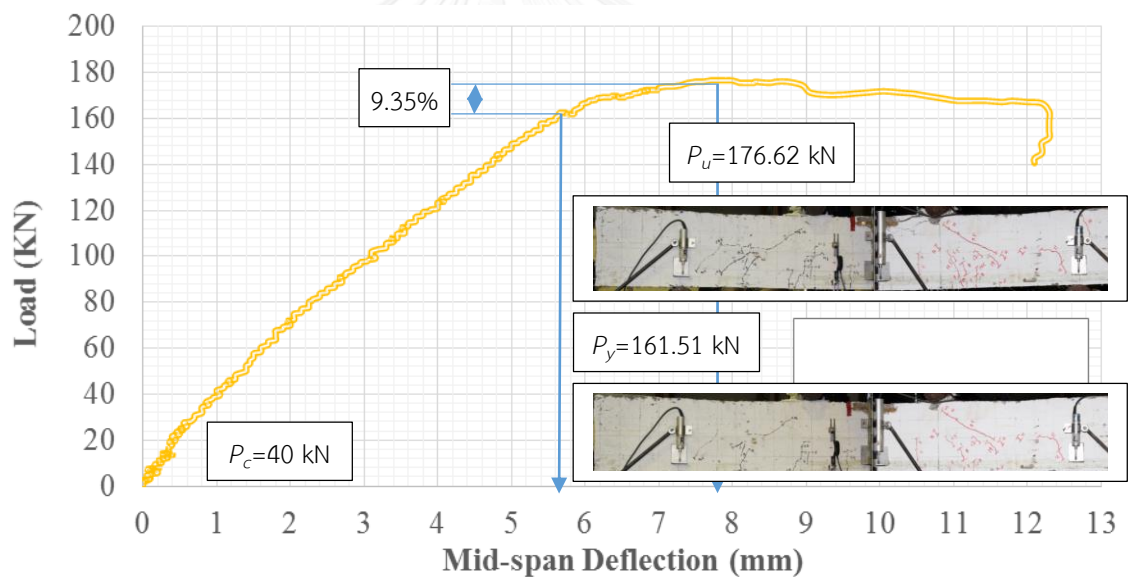


Figure 4.15 Load-midspan deflection behaviour of SB-AFM beam

For corroded beam and repairing by available product in market, SB-MP, the load deflection relationship is shown in **Fig. 4.16**. Beam SB-MP cracked at a load of 20 kN, yielded at a load of 133.9 kN, and failed at ultimate load of 152.65 kN with mid-span deflection of 0.45 mm, 5.1 mm, and 11.75 mm, respectively. There is increasing 23.62% from yielding to ultimate load.

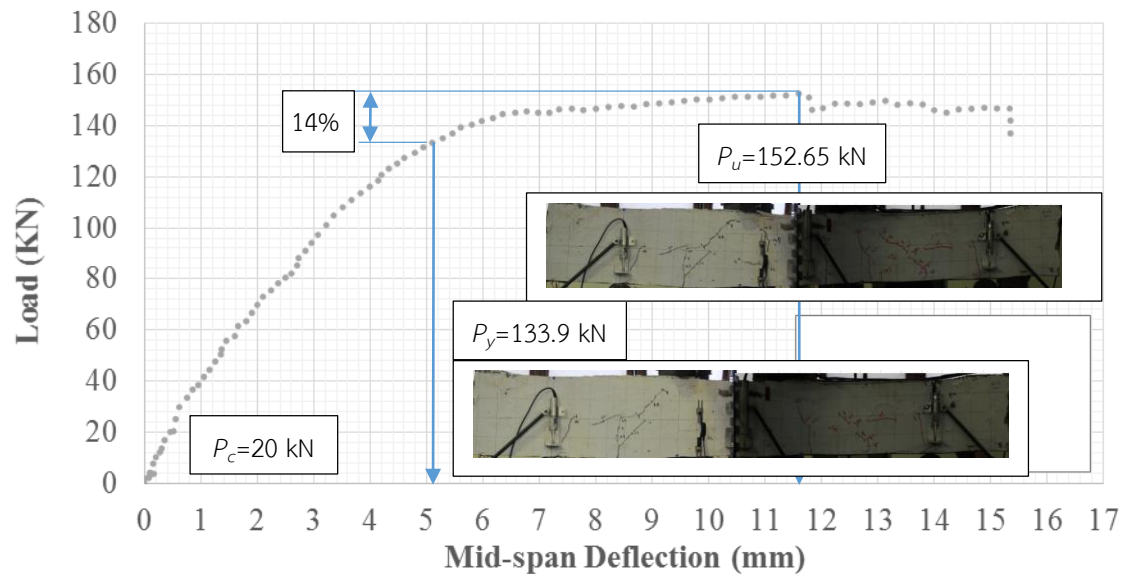


Figure 4.16 Load-midspan deflection behaviour of SB-MP beam

4.3.2.2 Ductility index

Displacement ductility was calculated as the ratio of the deflection at ultimate load, Δ_u , to the deflection at the yielding load for inelastic structure, Δ_y , is called the displacement ductility ratio. The result shows in **Table 4-12**.

Table 4-7 Displacement ductility

Beam ID	Deflection at the ultimate load (mm)	Deflection at the yielding load (mm)	Displacement ductility		
			$\mu = \Delta_u / \Delta_y$	$\mu / \mu_{(BC)}$	$\mu / \mu_{(NRB)}$
BC	7.40	4.45	1.66	1.00	-
NRB	6.55	3.55	1.84	1.11	1.00
SB-AFM	7.80	5.65	1.38	0.83	0.75
SB-MP	11.75	5.10	2.30	1.38	1.25

Where:

Δ_u : Displacement at ultimate load

Δ_y : Displacement at yield load

$\mu_{(BC)}$: The ratio of displacement at ultimate load to the displacement at yield load of BC beam.

$\mu_{(NRB)}$: The ratio of displacement at ultimate load to the displacement at yield load of NRB beam

For corroded beam without repairing, NRB, the displacement ductility ratio increases by 11% comparing with beam control.

For corroded beam repairing by aramid fibers mortar, SB-AFM, the displacement ductility ratio decreases by 17% comparing with beam control and decreases by 25% comparing with beam without repairing.

For corroded beam repairing by mortar product in the market, SB-MP, the displacement ductility ratio increases by 38% comparing with beam control and increases by 25% comparing with beam without repairing.

All of the section considered here was be under-reinforced. The meaning of an under-reinforced beam section is that, when the section is loaded in bending beyond its elastic range, the tension zone steel will yield before the concrete in the compression zone reaches its maximum useable strain, ϵ_{cu} . Corroded beam was yielded before control beam yielding, therefore, displacement ductility ratio of corroded beam is higher than control beam. However, there was effected by repaired material and breaking process. For SB-AFM, the yield load increases by 3% and displacement ductility ratio decreases by 25% comparing with beam without repairing. For SB-MP, although the yield load decreases by 15%, displacement ductility ratio increases by 25% comparing with beam without repairing.

4.3.2.3 Cracks pattern

There is two kinds of crack of BC beam, flexural cracks and flexure-shear cracks. Cracks are symmetric pattern with the middle line of beam as a line of symmetric. There are four main cracks for each side. Four flexural cracks occurred at load span.

Flexural cracks extend vertically into the beam. Two cracks occurred at each shear span side. Flexural cracks occurred first and extend less vertically into the beam. Crushing concrete occurred at the end of process.

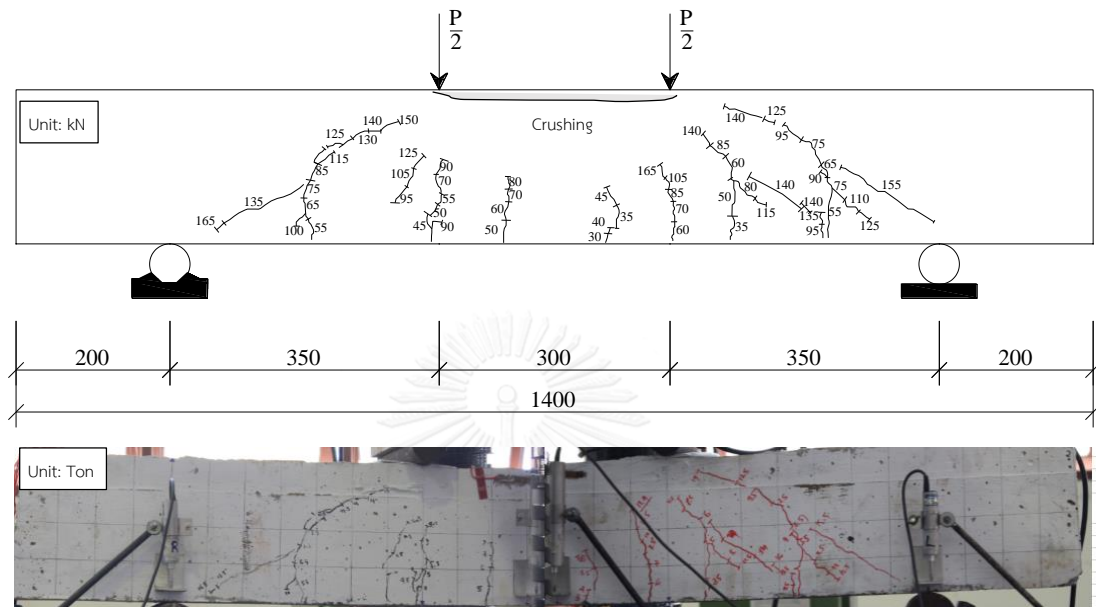


Figure 4.17 Cracks pattern of BC beam

For corroded beam without repairing, NRB, there is two kinds of crack. Flexural cracks extend vertically into the beam and flexure-shear cracks extend less vertically into the beam. There are two main cracks in the load span from beginning of process. From 100 kN, there has more three cracks at load span. There has one main incline crack at the left hand side and three incline cracks at the right hand side of shear span. Therefore, it may cause by the effect of corrosion on the beam. The corrosion effected ununiformed on longitudinal rebars. There is not symmetric by the middle line of beam. Crushing concrete occurred at the end of process.

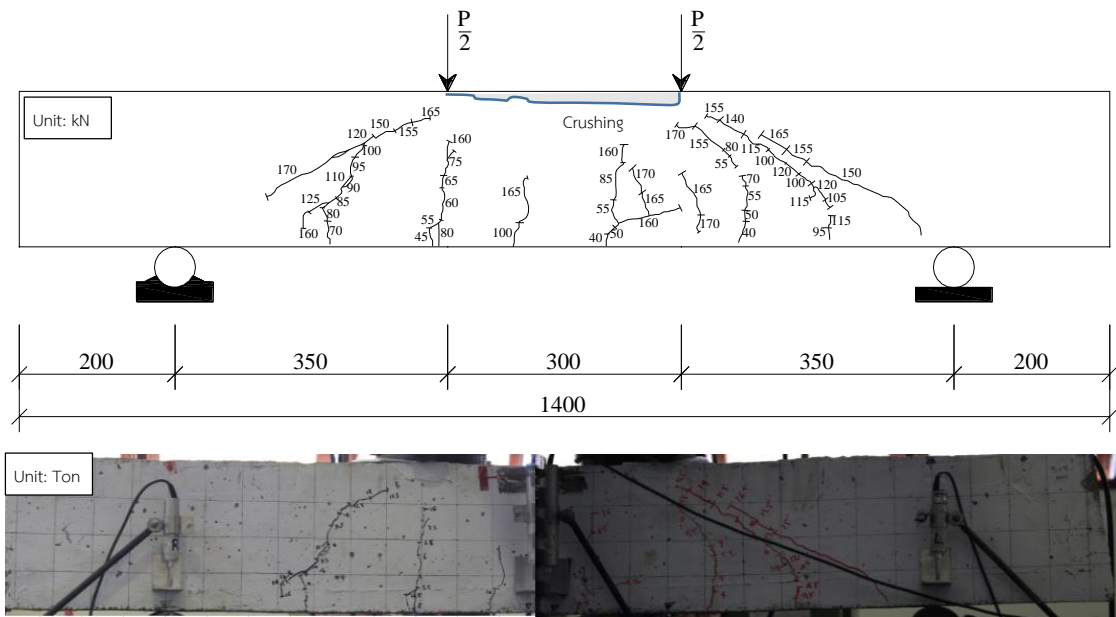


Figure 4.18 Cracks pattern of NRB beam

For corroded beam repairing by mortar in the market, cracks occurred at load span, shear span, bonding part, and support part. There are three main cracks at the load span.

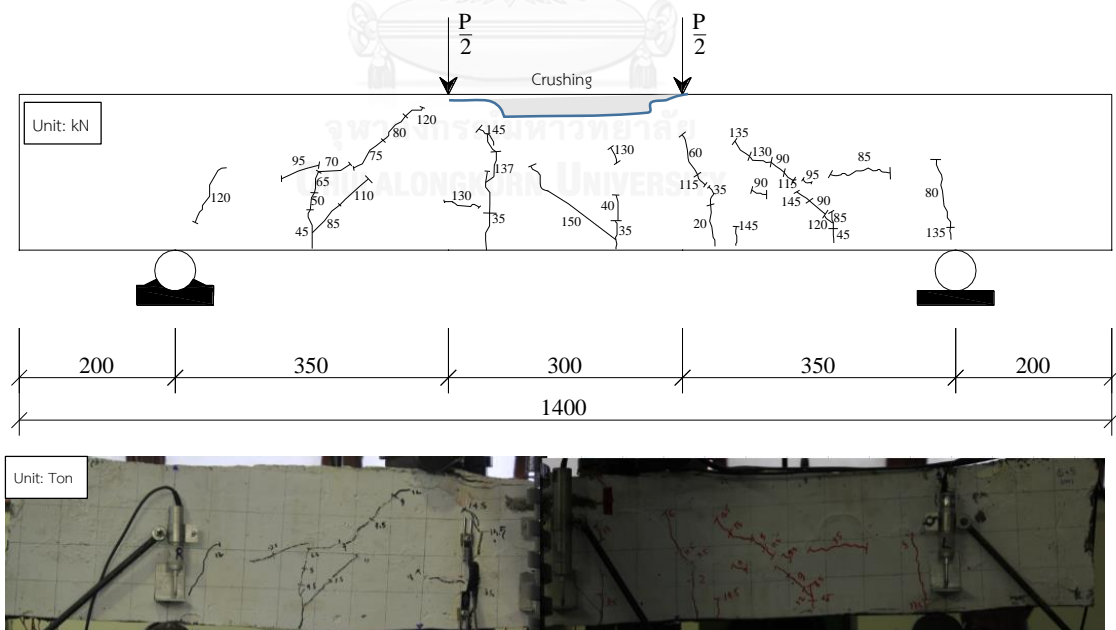


Figure 4.19 Cracks pattern of SB-MP beam

Especially, there has one larger incline crack which was occurred at 150 kN at load span of SB-MP beam. There has one incline crack at shear span and support for each side. Crack occurred at 120 kN, 85 kN at support and bonding part, respectively.

For corroded beam repairing by aramid fibers reinforced mortar, SB-AFM, many small cracks were observed. There are four main cracks at load span, two or three main cracks at shear span, and one crack at support part. Otherwise, there has one crack at compression strut as show in **Fig. 2.20**. Furthermore, cracks pattern of SB-AFM is more scattered than other beams.

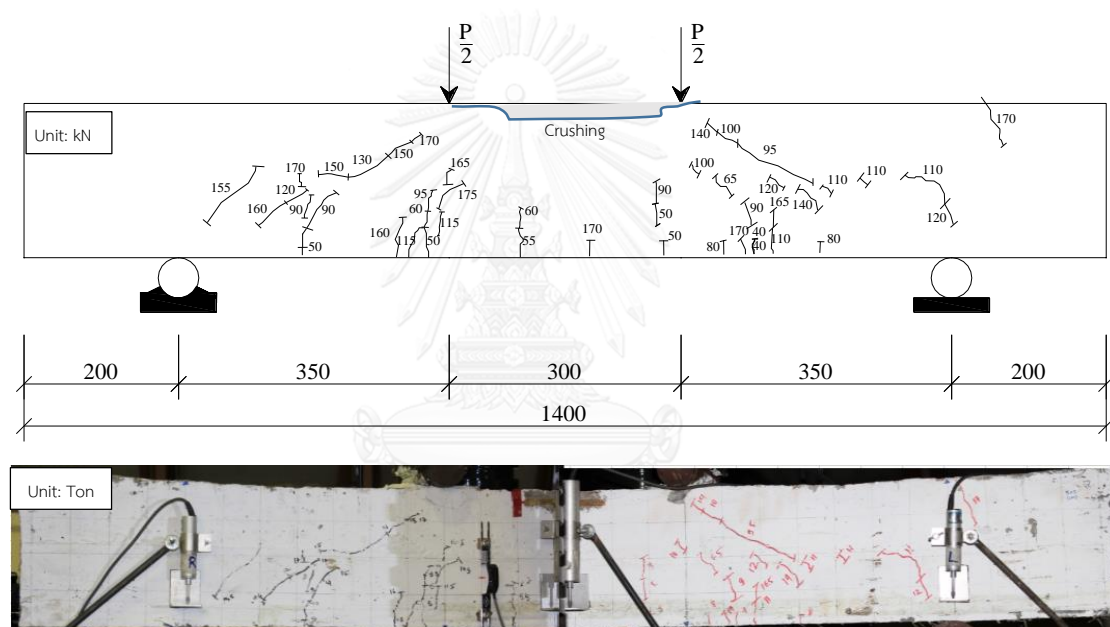


Figure 4.20 Cracks pattern of SB-AFM beam

4.3.2.4 Width of crack

The crack width of BC beam measured after testing is shown in **Fig. 4.21**. The maximum crack width is 4 mm at the middle part of the beam. Moreover, two flexural cracks at the point load has crack width of 2 mm and 2.5 mm. The crack width of incline crack is quite small (from 0.1 to 0.3 mm).

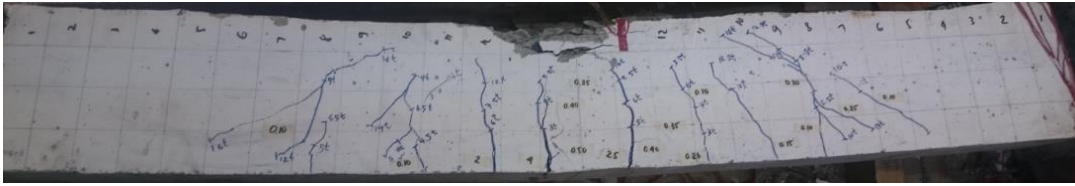


Figure 4.21 Crack width of BC beam (mm)

The crack width of NRB beam is shown in **Fig. 4.22**. The maximum crack width, 6 mm, was observed at the middle part of the beam. Moreover, there has a larger crack width, 3 mm, under point load at the right hand side of **Fig. 4.22**. However, at the other side of the beam under point load, the crack width 0.2 mm was observed. It may cause of effect of corrosion on reinforced concrete beam. It leads to resist the load non-uniformed at two side of the beam.

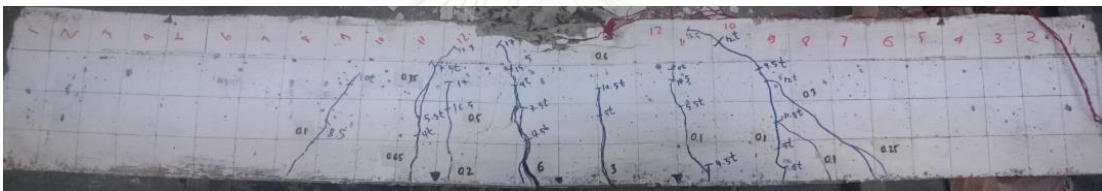


Figure 4.22 Crack width of NRB beam (mm)

The crack width of SB-AFM beam is shown in **Fig. 4.23**. The maximum width crack, 1.40 mm, was observed. The other crack width was observed from 0.20 mm to 0.40 mm. The SB-AFM occurred many small cracks. It may cause of presence of fibers in tension zone of the beam.

The crack width of SB-MP is shown in **Fig. 4.24**. The maximum width crack, 4 mm, was observed. The maximum width crack was observed at the middle and under point load of the beam. The larger incline cracks are main reason which lead to failure of SB-MP beam. Moreover, the other width cracks were 0.25 mm to 0.45 mm at shear span and 0.3 mm at bonding part.

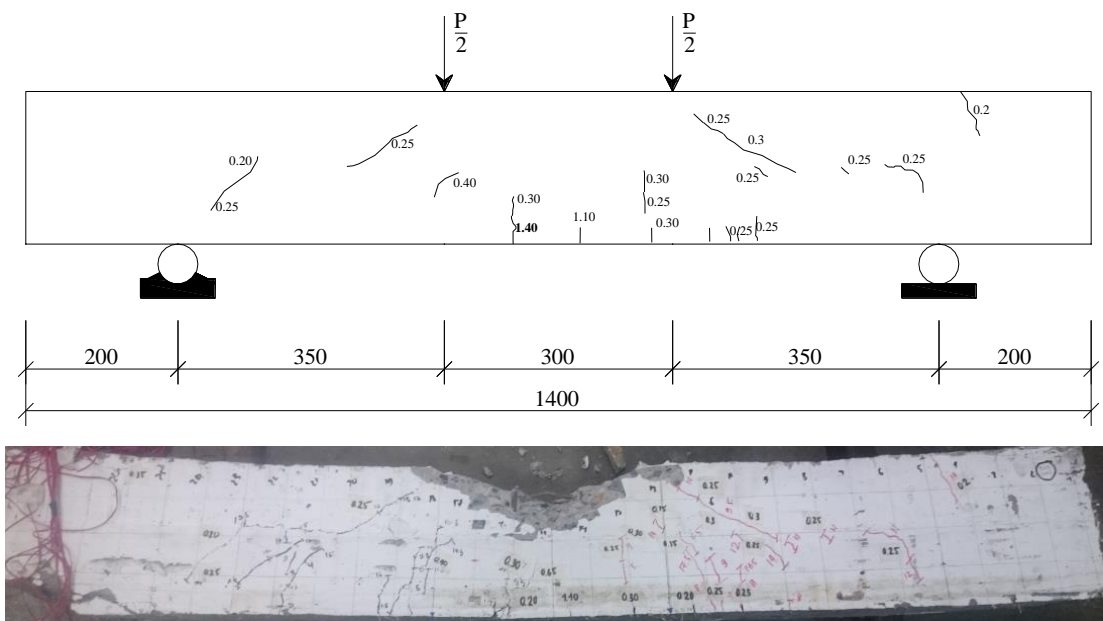


Figure 4.23 Crack width of SB-AFM beam (mm)

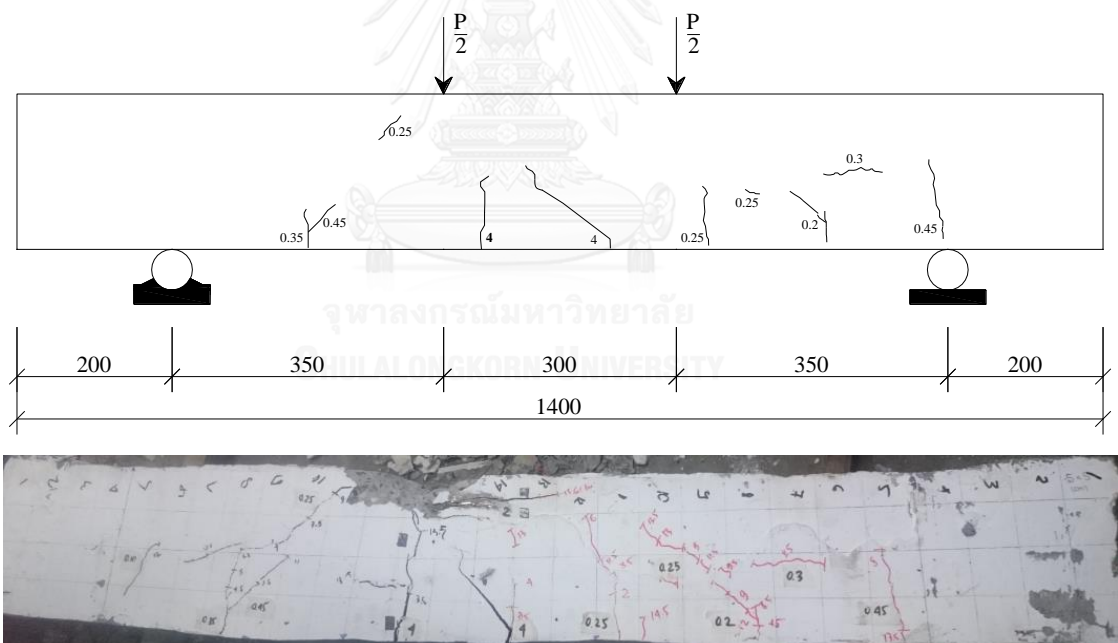


Figure 4.24 Crack width of SB-MP beam (mm)

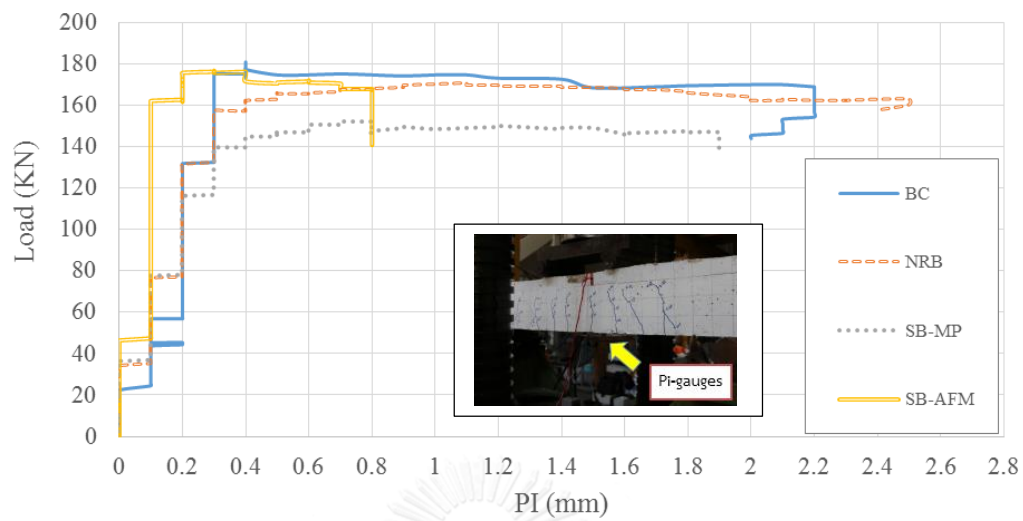


Figure 4.25 Crack width from Pi-gauges at the middle bottom soffit of the beams (mm)

Figure 4.25 shows the width cracks of pi-gauges at the middle bottom soffit of each beam. There is the same load-width crack relationship of four beams at the first stage (0 to 22 kN). SB-MP beam and NRB beam has the same load-width crack relationship at the second stage (38 kN to 117 kN). For SB-AFM beam, crack width significantly reduces. It may cause of presence of aramid fibers reinforced mortar in tension zone of the beam.

Chapter 5

PREDICTION OF FLEXURAL STRENGTH OF REPAIRING BEAMS

5.1 Assumptions

In order to predict the flexural behaviour of RC beams, a theoretical model using the sectional analysis method is presented in this section. The following assumptions are used for the analysis:

- 1) Sections perpendicular to the axis of bending that are plane before bending remain plain after bending.
- 2) The strain in the reinforcement is equal to the strain in the concrete at the same level.
- 3) The stresses in the concrete and reinforcement can be computed from the strains by using stress-strain curves for concrete and steel.
- 4) The tensile strength of conventional concrete will be ignored after cracking. However, the tensile strength of aramid fiber mortar could be used from direct tensile test.

5.2 Material model

The stress-strain relationship assumed for concrete in compression is shown in **Fig.5.1 (a)**. This model consists of a parabola from zero stress to the compressive strength of concrete, f'_c . The strain that corresponds to the peak compressive stress, ϵ_0 . The equation for this parabola, which was originally introduced by Hognestad, is

$$f_c = f'_c \left[2 \left(\frac{\epsilon_c}{\epsilon_0} \right) - \left(\frac{\epsilon_c}{\epsilon_0} \right)^2 \right] \quad (5-1)$$

In tension the conventional concrete is assumed to have a linear stress-strain relationship up to the concrete modulus of rupture, f_r .

A simple elastic-perfectly plastic model will be assumed for the reinforcing steel in tension or compression, as shown in **Fig.5.1 (b)**. The steel elastic modulus, E_s , is assumed to be 200,000 MPa. The material model for steel rebar is presented as:

$$f_s = \begin{cases} E_s \varepsilon_s & 0 \leq \varepsilon_s \leq \varepsilon_y \\ f_y & \varepsilon_s \geq \varepsilon_y \end{cases} \quad (5-2)$$

As seen from the above direct tensile test of aramid fibers mortar and previous assumption, the strain in the reinforcement is equal to the strain in the aramid fibers mortar at the same level, therefore, the stresses in the aramid fibers mortar can be computed from the strains in reinforcement by using stress-strain curves, as shown in **Fig.5.1 (c)**.

Fig.5.1 (d) presents the cross sections of convention RC beam and strengthened beam.

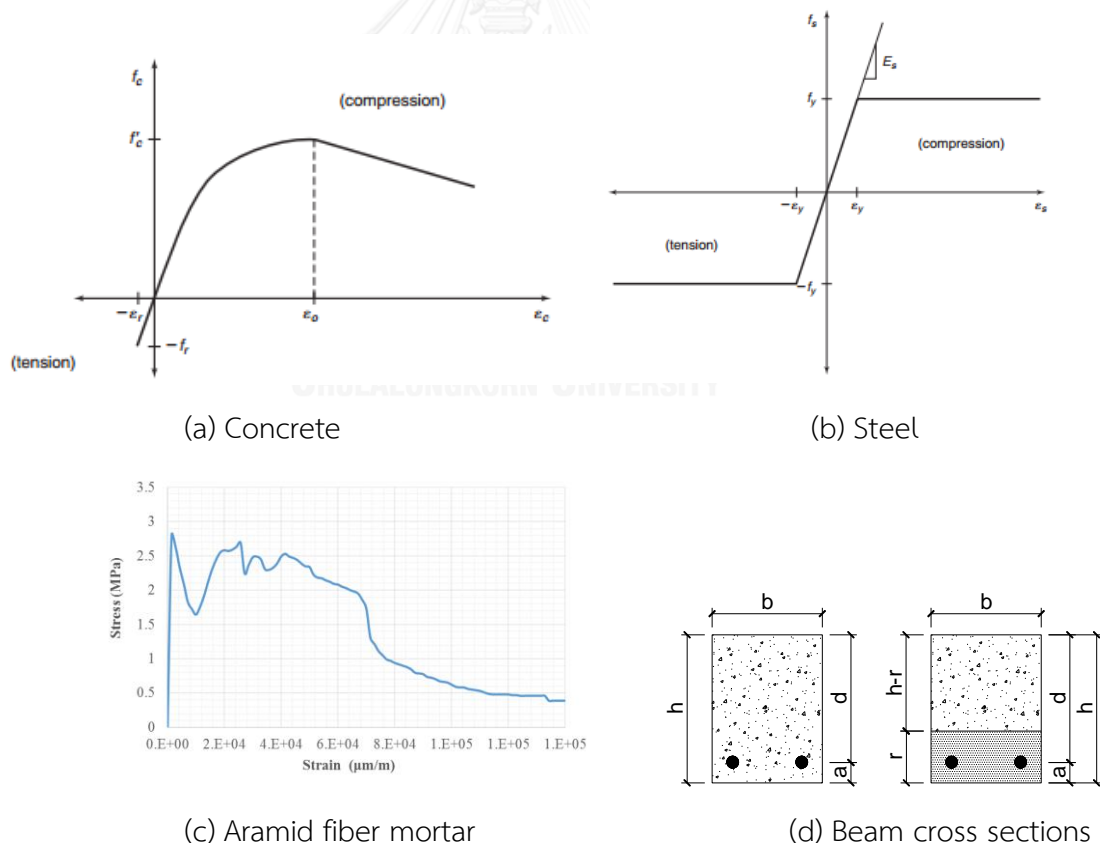


Figure 5.1 Material model for single reinforced concrete design

5.3 Methodology

Table 5-1 presented the material properties and values in the calculation. Figure 5.2 presents the stress-strain distribution of RC section for control beam and non-repairing beam. Unlike the conventional RC beams (Fig. 5.2), the stress-strain distribution at ultimate state of strengthened beam by AFRM is shown in Fig. 5.3. The tensile stress resisted by aramid fibers is taken into account. Cracking load and ultimate load of the beams were computed this chapter.

Table 5-1 Properties of material

No.	Parameter	Notation	Result	Unit
1	Compressive strength	f'_c	32	MPa
2	β_1	β_1	0.82	
3	Width of beam	b	150	mm
4	Height of beam	h	200	mm
5	Cover concrete	c	28	mm
6	The effective flexural depth	d	172	mm
7	Yield strength of reinforcement	f_y	537.15	MPa
8	Area of tension reinforcement	A_s	402	mm ²
9	Area of tension corroded reinforcement	A_s^*	358	mm ²
10	Young modulus of steel DB16 (SD40)	E_s	2E+05	MPa
11	Strain of steel at yield strength	ϵ_s	2685	$\mu\text{m}/\text{m}$
12	Shear span	a	350	mm
13	Strengthened depth	r	70	mm

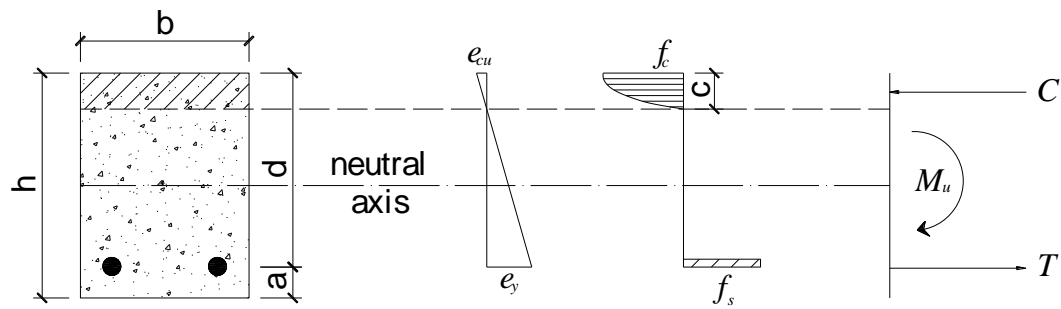


Figure 5.2 Stress-strain distribution at ultimate state of conventional beams

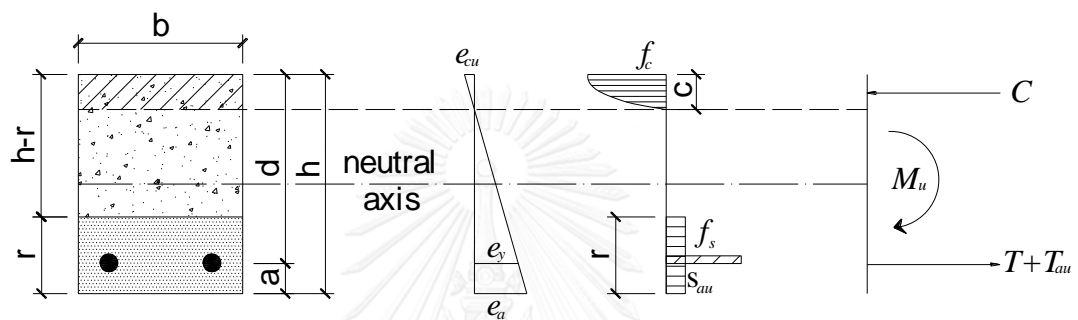


Figure 5.3 Stress-strain distribution at ultimate state of strengthened beam by AFRM

5.4 Calculation of cracking load

ACI code section 9.5.2.3 defines the modulus of rupture for use in the calculating deflection as

$$f_r = 0.62\lambda\sqrt{f'_c} = 0.62 \times 1 \times \sqrt{32} = 3.5 \text{ (MPa)} \quad (5-3)$$

Note that $\lambda=1.0$ for normal weight concrete.

The cracking moment is defined as the moment that causes the stress in the extreme tension fiber to reach the modulus of rupture,

$$M_{cr} = \frac{f_r I_g}{y_t} = \frac{3.5 \times \frac{1}{12} \times b \times h^3}{\frac{h}{2}} = \frac{3.5 \times \frac{1}{12} \times 150 \times 200^3}{\frac{200}{2}} = 3500 \text{ (kN.mm)} \quad (5-4)$$

$$P_{cr} = \frac{2M_{cr}}{a} = \frac{2 \times 3500}{350} = 20 \text{ (kN)} \quad (5-5)$$

While the moment of inertia for the gross section is defined as I_g , and the distance from the section centroid to the extreme tension fiber is defined as y_t .

From the load-strain relationship of four beams, approximate values for the cracking load are 18 to 20 kN which is close to the calculated results.

5.5 Calculation of ultimate flexural capacity

From similar triangles in the linear strain distribution in **Fig. 5.2** and **Fig. 5.3** the following expression can be derived:

$$\frac{\varepsilon_y}{d-c} = \frac{\varepsilon_c}{c} \quad (5-6)$$

$$c = \frac{\varepsilon_c d}{\varepsilon_y + \varepsilon_c} \quad (5-7)$$

The concrete compression force, C , is equal to the volume under the stress block. Whitney stress block is used here.

$$C = 0.85 f'_c b \beta_1 c \quad (5-8)$$

The steel strain exceeds the yield strain for ultimate state, the stress f_s in tension reinforcement equals the yield strength, f_y . The steel tension force:

$$T = A_s f_y \quad (5-9)$$

The assume stress distribution for aramid fibers reinforced mortar is given in **Fig. 5.3**. The stress block model in **Fig. 5.3** is used to replace the actual mortar stress distribution. A uniform tension stress, σ_a , shall be assumed distributed over an equivalent tension zone bounded the edges of the cross section and a straight line located parallel to neutral axis at the distance r from the mortar fiber. The strain in the longitudinal reinforcement is equal to the strain in the mortar at the same level. Therefore, the stress mortar shall be allowed the stress mortar by direct tensile test result and calculated from stress-strain relationship from direct tensile test as shown in **Fig. 5.1(c)**. The aramid fibers mortar tension force:

$$T_a = \sigma_a b r \quad (5-10)$$

Summing moment about the centroid of beam cross section gives the following results:

The moment caused by concrete compression force:

$$M_c = C \left[\frac{h}{2} - \frac{\beta_1 c}{2} \right] \quad (5-11)$$

The moment caused by steel tension force:

$$M_T = T \left[d - \frac{h}{2} \right] \quad (5-12)$$

The moment caused by aramid fibers mortar tension force:

$$M_{T_a} = T \left[\frac{h}{2} - \frac{r}{2} \right] \quad (5-13)$$

The nominal moment strength at the centroid of beam cross section will be:

$$M_n = M_c + M_T + M_{T_a} \quad (5-14)$$

Results obtained from beam testing and those calculated using the model are summarized in **Table 5-2**.

Table 5-2 Comparison ultimate load of modelling and experimental results

Beam ID	Modelling				Experiment		Comparison
	M_c (kN.m)	M_T (kN.m)	M_{T_a} (kN.m)	M_n (kN.m)	Load (kN)	M_e (kN.m)	M_n/M_e
BC	16.2	15.5	-	31.7	180.79	31.6	1.00
NRB	17.2	13.8	-	31	170.37	29.8	1.04
SB-AFM	14.6	13.8	1.84	30.24	176.62	30.9	0.98
SB-MP	11.1	13.8	-	24.9	152.65	26.7	0.93
Mean ratio							0.99

The moment prediction of the corroded beam without repairing is higher than the experimental moment. It may have caused by the bonding between reinforced rebars and concrete. The occurring of corrosion induced-cracking lead to decreases

bond strength. Therefore, the decreasing bond strength affected on the result of prediction modelling. However, the corroded beam repairing by aramid fiber mortar and mortar product in the market was soaked in diammonium hydrogen citrate for 2 days to clean the rust around reinforced bars. Therefore, the bond strength was unaffected on the result of prediction modelling.

The calculated moment shows good agreement with the experimental results. Therefore, the calculation proposed in this study can be used to predict the flexural capacity of corroded RC beam and the repaired beam.



Chapter 6

CONCLUSION AND RECOMMENDATION

6.1 Experiment Result

6.1.1 Mechanical properties AFRC test

From the mechanical properties of aramid fibers reinforced concrete results, the following conclusions can be drawn:

1. There is no significant effect of fiber geometry on the compressive strength and splitting strength of aramid fiber reinforced concrete (AFRC). However, there is improvement in splitting tensile strength with the appearance of aramid fiber in concrete.
2. There are two failure modes observed in the specimens including rupture and pull-out. The failure mode depends on the length and shape of fibers. Although aramid fiber is outstanding in tensile strength, aramid fibers were ruptured while tensile stress was around 1.5 to 2.95 MPa. It may cause by the difference of the resistance load which each filaments resists. Each filament ruptured first and led to totally fiber ruptured.
3. Fiber with 30 mm long are not be able to provide the sufficient embedded length in the concrete because the fibers mainly pulled-out at the peak load. Fiber with 50 mm long showed relatively lower tensile strength from the direct tensile test because of fiber balling. With the increase in fiber length, workability of concrete decreased and balling of fibers occurred. Forty-mm is the proper fiber length to increase the tensile strength of aramid fiber reinforced concrete. Although the single shape fibers yield the highest peak tensile stress, twist fibers can resist higher loads in post-peak region.

6.1.2 Flexural behaviour of reinforced concrete beam

From the bending test four-point load of beams results, the following conclusions can be drawn:

1. The beam reduces 10% mass loss of reinforced rebar lead to reduce 6% of load capacity and 12% of the deflection at the ultimate load.
2. Repairing corroded RC beams with 1.0% of aramid fibers reinforced mortar can slightly increase load capacity about 3% comparing with the corroded beam without repairing. The load capacity was recovered to be close to the non-corroded RC beams. By using the aramid fiber reinforced mortar can be slightly delayed the yielding of longitudinal reinforcement. In addition, the number of cracks increases in corroded beam repairing by aramid fibers mortar, however, the width of cracks decreases significantly.
3. The flexural capacity of corroded beam repaired by mortar product in the market decreased 11% comparing with the corroded beam without repairing. The wide crack width was found before the ultimate stage leading the early yielding of steel reinforcement. Using only mortar cannot recover the flexural capacity of the corroded RC beam.
4. A model for predicting the ultimate flexural capacity of beams is suggested. The model considers the fiber contribution to concrete in tension. The occurring of corrosion induced-cracking lead to decreases bond strength. The decreasing bond strength affected on the result of prediction modelling. Therefore, the moment prediction of the corroded beam without repairing is higher than the experimental moment. However, the results from predicted model are found to agree well with test data obtained. It demonstrates that the suggested model can be used to predict the ultimate flexural capacity of beams accurately.

6.2 Recommendations for future work

For future work study, it is recommended to:

- To obtain the effect of aramid fibers reinforced concrete in shear capacity
- To obtain the effect of aramid fibers reinforced concrete in natural corrosion.
- Modelling of corroded reinforced concrete beams should be performed to compare the results and finite element analysis by using simulation software.



References

1. Search. *Products of Aramid fiber*. 2015; Available from: <http://www.dupont.com/products-and-services/fabrics-fibers-nonwovens/fibers/brands/kevlar.view-all.hlm-usesapplications-usesapplication.html>.
2. 544, A.C. *State-of-the-Art Report on Fiber Reinforced Concrete*. in *ACI Journal Proceedings*. 1973. ACI.
3. Search. *Properties of Aramid fibers*. 2015; Available from: http://www.christinedemerchant.com/aramid_characteristics.html.
4. El Maaddawy, T., K. Soudki, and T. Topper, *Long-term performance of corrosion-damaged reinforced concrete beams*. *ACI Structural Journal*, 2005(102): p. 649-656.
5. Pereira, E., et al., *Chloride accelerated test: Influence of silica fume, water/binder ratio and concrete cover thickness*. *Revista IBRACON de Estruturas e Materiais*, 2013. **6**(4): p. 561-581.
6. El Maaddawy, T., K. Soudki, and T. Topper, *Long-term performance of corrosion-damaged reinforced concrete beams*. *ACI Structural Journal*, 2005. **102**(5): p. 649.
7. Amleh, L. and S. Mirza, *Corrosion influence on bond between steel and concrete*. *Structural Journal*, 1999. **96**(3): p. 415-423.
8. Wei-liang, J. and Z. Yu-xi, *Effect of corrosion on bond behavior and bending strength of reinforced concrete beams*. *Journal of Zhejiang University SCIENCE*, 2001. **2**(3): p. 298-308.
9. Nakamura, H., et al. *Crack propagation analysis due to rebar corrosion*. in *Proceedings of the 7th International Conference on Fracture Mechanics of Concrete and Concrete Structures (FramCoS-7)*, Korea. 2010.
10. Berrocal, C.G., *Chloride Induced Corrosion of Steel Bars in Fibre Reinforced Concrete*. 2015.
11. YUAN, H., et al., *Research on the tensile mechanics properties of steel fiber RPC*. 2015.

12. Lampropoulos, A., et al., *Strengthening of reinforced concrete beams using ultra high performance fibre reinforced concrete (UHPFRC)*. Engineering Structures, 2016. **106**: p. 370-384.
13. Uchida, Y., T. Takeyama, and T. Dei, *Ultra high strength fiber reinforced concrete using aramid fiber*. Proceedings of Fracture Mechanics of Concrete and Concrete Structures–High Performance, Fiber Reinforced Concrete, Special Loadings and Structural Applications, 2010: p. 1492-1494.
14. Iqbal, S., et al., *Strengthening of RC beams using steel fiber reinforced high strength lightweight self-compacting concrete (SHLSCC) and their strength predictions*. Materials & Design, 2016. **100**: p. 37-46.
15. MacGregor, J.G., et al., *Reinforced concrete: mechanics and design*. Vol. 3. 1997: Prentice Hall Upper Saddle River, NJ.
16. Ning, X., et al., *Experimental study and prediction model for flexural behavior of reinforced SCC beam containing steel fibers*. Construction and Building Materials, 2015. **93**: p. 644-653.
17. Swamy, R. *Deformation and ultimate strength in flexure of reinforced concrete beams made with steel fiber concrete*. in *ACI Journal Proceedings*. 1981. ACI.
18. Stroeven, P. and J. Hu, *Effectiveness near boundaries of fibre reinforcement in concrete*. Materials and structures, 2006. **39**(10): p. 1001-1013.
19. Materials, A.S.f.T. *Standard Test Method for Compressive Strength of Cylindrical Concrete Specimens*. 2015. American Society for Testing and Materials Philadelphia, PA, USA.
20. Norma, A., *C496/C496M-11, Standard test method for splitting tensile strength of cylindrical concrete specimens*. C.
21. Rokugo, K., et al., *Applications and recommendations of high performance fiber reinforced cement composites with multiple fine cracking (HPFRCC) in Japan*. Materials and structures, 2009. **42**(9): p. 1197-1208.
22. Naaman, A.E., *Engineered steel fibers with optimal properties for reinforcement of cement composites*. Journal of Advanced Concrete Technology, 2003. **1**(3): p. 241-252.

23. Batson, G. *State-Of-The-Art Report on fiber reinforced concrete*. 1973. American Concrete Institute.



REFERENCES



APPENDIX



VITA



